Mathematics and Computers in Simulation 245 (2026) 530–552

Contents lists available at ScienceDirect

Mathematics and Computers in Simulation

journal homepage: www.elsevier.com/locate/matcom

Original articles

A modeling framework to strengthen the discrimination of unnecessary air traffic ground regulations by assessing overloaded sector dynamic behavior

Alfons Borràs [a],*, Laura Calvet [a], Miquel Àngel Piera [a], Gabriella Gigante [b]

[a] Department of Telecommunications and Systems Engineering, Autonomous University of Barcelona (UAB), Carrer Emprius, 2, 08202, Sabadell, Barcelona, Spain
[b] Centro Italiano Ricerche Aerospaziali (CIRA), Via Maiorise s.n.c., 81043, Capua (CE), Italy

ARTICLE INFO

Keywords:
Airspace sector capacity
Aircraft early handover (CAEHO)
Air traffic flow modeling
Nonlinear eligibility model

ABSTRACT

Air Traffic Flow and Capacity Management (ATFCM) aims to balance traffic demand and sector capacity while maintaining safety and network performance. When tactical measures such as rerouting or sector reconfiguration are insufficient to meet demand, ground regulations are imposed as a last resort, generating delays. As an alternative capacity-on-demand mechanism, Clusterized Aircraft Early Handover (CAEHO) enables the early transfer of clustered aircraft near sector boundaries to adjacent sectors with available capacity.

This paper introduces a modeling framework to support tactical CAEHO deployment decisions in overload situations where small variations in traffic distribution can lead to markedly different operational outcomes. A macroscopic model describes the spatiotemporal evolution of aircraft density within a sector, while a nonlinear eligibility formulation characterizes aircraft clustering through a power-law representation governed by the exponent α. This exponent reflects the nonlinear relationship between traffic organization and early handover feasibility and is driven by the internal spatial distribution of traffic. Sector-level characteristics such as baseline occupancy (offset), mean dwell time, and peak load are used to approximate its value, while uncertainty in planned traffic induces a range of possible α estimates.

The proposed framework is validated using synthetic scenarios and real-traffic-driven simulations over the European airspace. The results show that the exponent α exhibits consistent discriminative behavior with respect to CAEHO feasibility under realistic sector overload conditions, particularly under limited remaining dwell time.

The resulting feasibility indicator provides sector-level decision support to assess whether CAEHO can safely avoid an Air Traffic Controller–capacity regulation during the tactical phase.

1. Introduction

Airspace is divided into sectors to ensure that Air Traffic Controllers (ATCo's) can manage aircraft flows safely and efficiently [1]. Each sector defines a portion of the airspace for which a pair of ATCo's, typically an executive and a planner, are responsible [2]. A review of different approaches to airspace sectorization can be found in [3]. These approaches aim to determine sector configurations that account for traffic demand while ensuring that the number of aircraft simultaneously present in a sector does not exceed a predefined occupancy-based capacity threshold [4]. Since traffic demand varies significantly over the day, sector

* Corresponding author.
E-mail address: Alfons.Borras@autonoma.cat (A. Borràs).

https://doi.org/10.1016/j.matcom.2026.02.022
Received 11 July 2025; Received in revised form 9 February 2026; Accepted 18 February 2026
Available online 19 February 2026

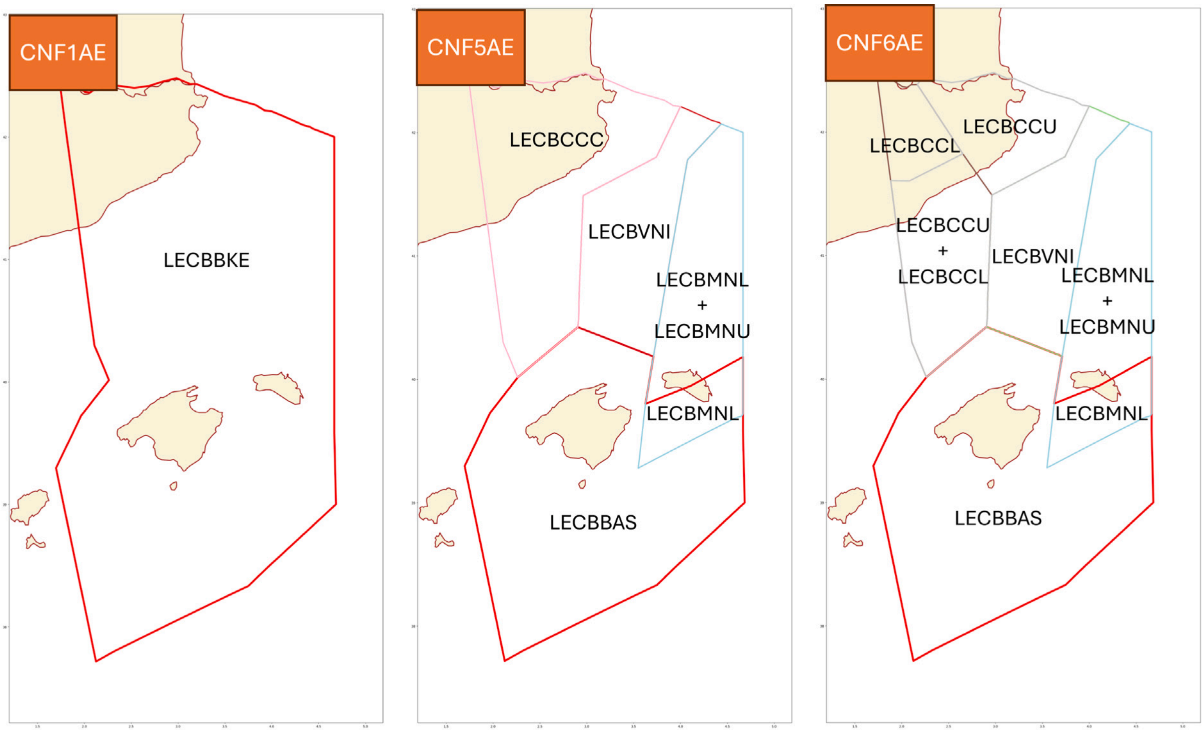

(a) CNF1AE configuration (00:00–04:19) (b) CNF5AE configuration (06:00–17:59) (c) CNF6AE configuration (18:00–19:59)

Fig. 1. LECBCTAE ACC sample of configurations.

configurations are often adjusted dynamically by activating or deactivating sectors in order to better match demand with available capacity [5].

To illustrate how sectorization evolves dynamically throughout the day, Fig. 1 presents representative sector configurations for the LECBCTAE Area Control Centre (ACC) on 27 July 2024. As traffic demand increases, the ACC is progressively split into a larger number of sectors in order to better match demand with available capacity. Fig. 1(a) depicts the nighttime configuration (00:00–04:19), in which the ACC operates as a single sector (LECBBKE). During the daytime peak period (06:00–17:59), shown in Fig. 1(b), the ACC is subdivided into five sectors (LECBBAS, LECBMNL, LECBMNU, LECBVNI, and LECBCCC) to accommodate higher traffic levels. Finally, as demand continues to increase in the early evening, Fig. 1(c) illustrates a further refinement of the configuration (18:00–19:59), in which the ACC is split into six sectors (LECBBAS, LECBMNL, LECBMNU, LECBVNI, LECBCCU, and LECBCCL). Some sectors may partially overlap in their horizontal projections but are separated by distinct flight level boundaries, for example LECBMNL and LECBMNU, or LECBCCU and LECBCCL.

Unfortunately, despite there are several mathematical solutions to set the optimal configuration of sectors, these solutions cannot be implemented at practical level due to the fast pace time-variant dynamic characteristics of traffic demand which cannot be counterbalanced by the rigidity (technical, staff or set-up time requirements) of low pace airspace capacity mechanisms diming the possibility to implement efficient and effective "capacity-on-demand" measures where and when they are needed [6,7]. Note that a small departure delay of a reduced set of aircraft in different airports, could easily lead to an increment of the amount of aircraft in a sector at a given time above accepted capacity values, rising safety issues due to ATCo overload operational contexts [8].

Air Traffic Flow and Capacity Management (ATFCM) is enhanced through a set of advanced services to define, on the day prior to operations, the best sector configuration according to the planned traffic demand and formalize the ADP (Air Traffic Management daily plan) with the scheduling of the active sectors to be activated by the different Air Navigation Service Providers (ANSPs). However, during the day of operations, imbalances between the latest estimates of sector-level traffic demand and the available capacity are initially addressed through tactical coordination aimed at rebalancing demand and capacity. If capacity cannot be adjusted sufficiently within the required time scale, ATFCM interventions necessarily concentrate on demand restraint, most commonly through the application of Short-Term ATFCM Measures (STAM) [9]. Fig. 2 illustrates the different ATFCM phases to avoid demand-capacity unbalances (NOP stands for Network Operations Plan).

Among the different ATFCM measures to tackle the air traffic demand at sector level during the day of operation, the most common mechanism is ground regulation in which some aircraft departures are delayed a certain amount of time at the airports according to the CASA algorithm [10]. In this context, such ground delays constitute what are commonly referred to as Air Traffic Control (ATC) capacity regulations, which are deployed when sector demand is expected to exceed available operational resources and cannot be absorbed through capacity adjustments alone.

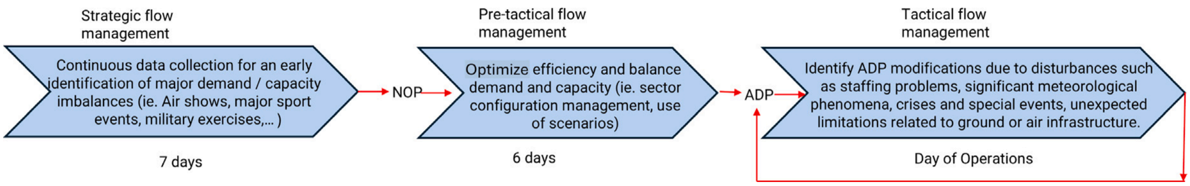

Fig. 2. ATFCM phases.

According to EUROCONTROL [11], in 2024, total en-route delay amounted to 22,385,540 min. Of this total, ATC-capacity regulations accounted for 8,691,028 min (approximately 39%), weather-related delays contributed 8,113,537 min (about 36%), ATC-staffing shortages caused 2,913,709 min (around 13%), and other causes made up 2,667,266 min (approximately 12%). Notably, ATC-capacity regulations alone contributed nearly 40% of total en-route delays during 2024.

The economic impact of these delays is substantial. Considering an average ATFCM delay cost of approximately 100 € per minute [12], the total en-route ATFCM delay in 2024 implies annual delay costs to airspace users that exceed €2.2 billion, only in Europe. ATC-capacity-related regulations alone would account for nearly €870 million in direct delay costs each year, although there is, however, no direct linear relation between delay and cost of the delay and the impact could not be the same depending on different space regions [13]. These figures illustrate the high financial burden of flow restrictions on airlines, passengers, and the wider aviation industry.

Several research projects try to mitigate the demand-capacity unbalances in the day of operations by improving airspace capacity rather than affecting traffic demand, such as Dynamic Airspace Sectorization (DAS), Dynamic Airspace Configuration (DAC), and Flight-Centric Airspace (FCA) procedures [1,3,14]. Among these, DAC currently appears to be the most mature candidate for full implementation, as it enables sectorization boundaries to be flexibly and dynamically adjusted according to time-varying traffic demand. The DAC solution specifically targets the INAP (Integrated Network Management and Air Traffic Control Planning) phase [15], covering the pre-tactical timeframe from six hours to fifteen minutes prior to operations, with threshold parameters adaptable to local operational constraints. However, advanced DAC solutions are still at research level, and its deployment will require non cost-efficient changes and overcome some barriers, such as it is the case of a system ATCo license [16] for virtual centers.

Related data-driven coordination and monitoring approaches have also been explored in other traffic domains, particularly in urban road networks and intersection-level management, although these operate at different spatial and operational scales than en-route ATFCM [17–19].

An alternative approach to implement a "capacity-on-demand" measure at the operational level is pursued within the ANTICIPATE project [20] through the Clusterized Aircraft Early Handover (CAEHO) mechanism, initially introduced in [21]. The core idea of CAEHO is to anticipate the transfer of control responsibility for selected aircraft located near the exit boundary of an overloaded sector, reallocating part of the control task to adjacent sectors with available spare capacity. By reducing the effective occupancy of the overloaded sector at critical moments, CAEHO may mitigate peak load situations and, in some cases, reduce the need for ground flow regulations due to ATC-capacity constrains.

From an ATFCM perspective, the CAEHO mechanism is explicitly aligned with the objective of improving airspace network efficiency, understood as the ability of the ATM network to accommodate traffic demand while minimizing delay, inefficiency, and unnecessary resource consumption, in accordance with the SESAR Performance Framework [22].

Subsequent studies have examined the feasibility of this concept under realistic operational assumptions. In [23], the potential impact of early handover on ATCo workload and sector throughput is analyzed, indicating that early delegation can be beneficial when applied selectively and under well-defined conditions.

In this context, CAEHO is assumed to apply only to a restricted subset of aircraft, subject to basic eligibility conditions at the time of transfer, including the absence of unresolved conflicts and a bounded remaining dwell time to the sector exit to ensure that the handover remains temporally meaningful [24].

CAEHO is not intended to operate within Terminal Control Areas (TCAs), also commonly referred to in the literature as Terminal Maneuvering Areas (TMAs), which are airport-centric airspace volumes primarily dedicated to arrival and departure flows [25]. Traffic within TMAs is characterized by frequent climb and descent phases, significant speed and altitude variability, and strong coupling with runway operations [26], making early handover impractical and operationally undesirable. Accordingly, the CAEHO mechanism is restricted to en-route sectors, typically above FL240, where aircraft operate predominantly in cruise conditions. In this regime, aircraft fly at quasi-steady Mach numbers, and en-route speed variations remain bounded around a nominal cruise value. As shown in the literature, such variations can be represented as limited deviations about an average link speed [27], with a negligible impact on macroscopic quantities such as remaining dwell time, thereby supporting a quasi-steady modeling assumption for CAEHO eligibility assessment.

Although CAEHO introduces additional coordination procedures between adjacent sectors, these requirements are deliberately constrained to ensure that early handover remains operationally useful, feasible, and safe, while preserving compatibility with existing ATC separation, conflict detection, and coordination frameworks.

More recently, these assumptions and their implications for coordination and workload redistribution have been discussed in a conference contribution presented at SESAR Innovation Days 2025 [24], where CAEHO is positioned as a tactical, human-centered

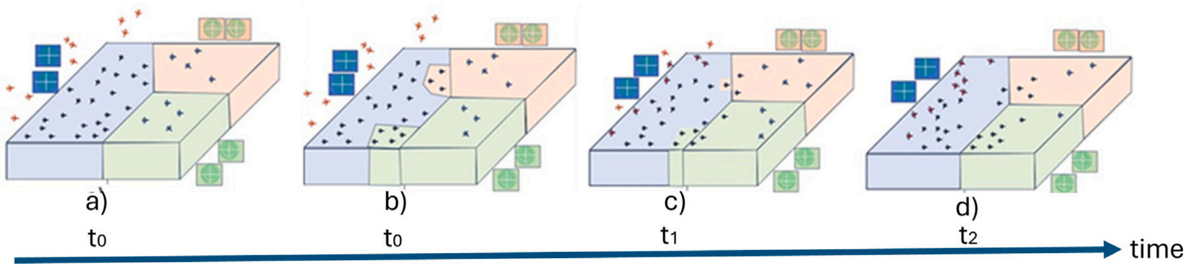

Fig. 3. CAEHO concept.

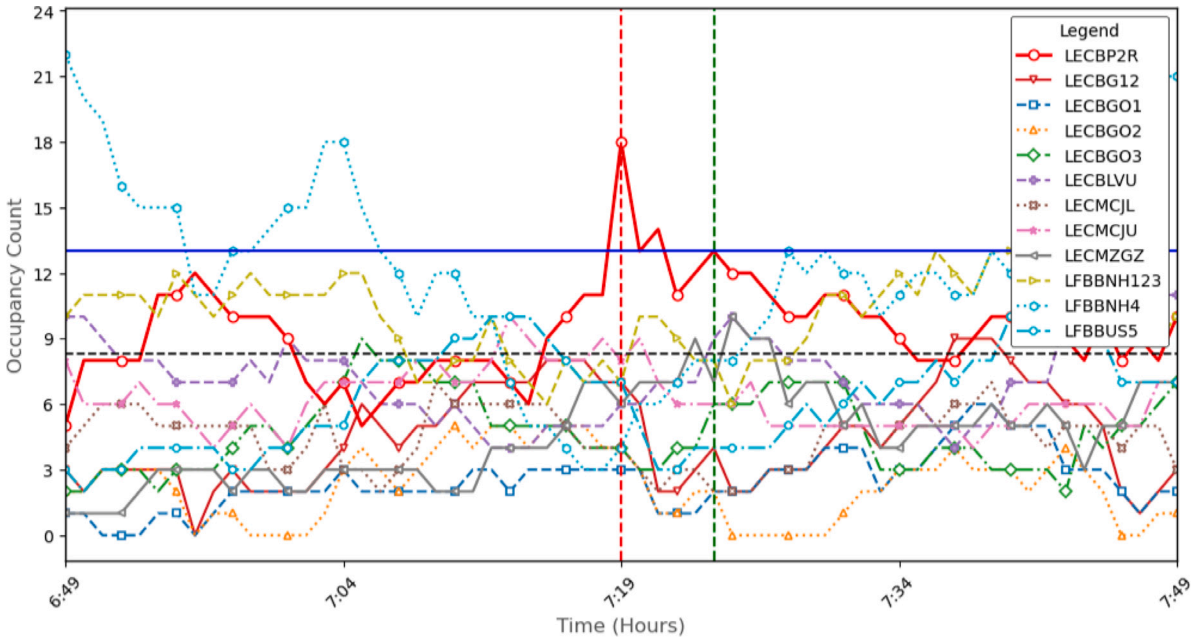

Fig. 4. LECBP2R occupancy count levels when regulated and its adjacents.

mechanism that operates within the existing ATFCM framework to actively mitigate sector overloads and, when feasible, reduce or avoid the application of ATC-capacity regulations.

Fig. 3 illustrates the operational concept of the CAEHO mechanism. In Fig. 3a, the blue sector is about to become overloaded as additional aircraft are projected to enter, pushing demand beyond its certified occupancy count limit at time t_0. It is important to note that the adjacent green and pink sectors still have spare capacity, as indicated by their lower occupancy count levels. At the same moment (t_0), the CAEHO mechanism is activated, transferring the control of selected aircraft from the overloaded blue sector to the neighboring green and pink sectors (Fig. 3b). This early transfer reduces the occupancy of the blue sector, creating capacity for inbound aircraft that would otherwise trigger an overload. Fig. 3c shows the clusterized aircraft physically progressing into the adjacent downstream sectors, and by Fig. 3d the transfer is fully completed, demonstrating the effective redistribution of demand and workload across the control area.

Obviously, the CAEHO mechanism requires the availability of spare capacity to be fully effective, which means that when an overloaded sector exceeds its occupancy level threshold, its adjacent sectors must maintain occupancy levels below their own limits. In this context, Fig. 4 illustrates the occupancy count of the LECBP2R sector (continuous red line with hollow circular markers), which exceeds its maximum allowed occupancy level (horizontal blue line), while the occupancies of its adjacent sectors remain well below that level at the moment when the CAEHO mechanism needs to be triggered (vertical red-dotted line). The horizontal black dotted line indicates the offset level, defined as the baseline sector occupancy preceding the congestion peak. As explained in Section 5, the spare capacity available within the European Civil Aviation Conference (ECAC) area [28] was sufficient to prevent 97% of the overloading peaks that could otherwise have resulted in the application of ground regulations, although some requirements may reduce the overall performance of the mechanism (conflict detection among aircraft, and remaining dwell time to the downstream sector, for example). In the remaining cases, alternative STAM measures may still be applied, albeit typically with higher operational impact than CAEHO-based delegation.

The advantage of CAEHO is that can be applied at the very last moment before the occupancy count of a sector could rise above the sector capacity, when traffic demand at sector level is well known, since aircraft are just less than 5 min to the entry sector waypoints. However, this timeliness advantage at operational level, can be seen as the main threat of the capacity-on-demand mechanism, since there are no last alternative solution to avoid sector overload, in case there are no enough CAEHO aircraft candidates (ie. aircraft located near the exit sector waypoints).

In this context, the present work focuses on providing sector-level information to support ATFCM decision-making under dynamically changing traffic conditions. The proposed framework aims to characterize how the distribution of traffic within a sector influences the availability of aircraft near the exit boundary, which is a key prerequisite for the feasible application of the CAEHO mechanism.

The approach first presents a physically consistent conservation law to model the spatiotemporal evolution of aircraft density within a sector from an Eulerian perspective. In parallel, a nonlinear, dwell-time-based eligibility model is developed using a Bernoulli-type ordinary differential equation (ODE), which estimates the amount of aircraft candidates near the sector exit. A normalized power-law representation governed by an exponent α is derived, serving as an intuitive indicator of clustering intensity and handover readiness. Importantly, it is demonstrated – using both synthetic and real-world data – that α can serve as a valuable indicator of the likely feasibility of CAEHO and can be influenced by sector-level parameters. This makes it possible to perform an initial qualitative assessment of CAEHO success using only basic sector information, thereby avoiding the need for complex, large-scale trajectory processing. The proposed framework is therefore intended as an ATFCM decision-support tool to discriminate those sectors where the CAEHO mechanism could be applied, avoiding unnecessary ground regulation measures.

The paper is organized as follows. First, a brief overview of the state of the art in air traffic flow modeling is provided. The proposed framework is then introduced and its main components are described. Finally, the approach is validated using synthetic and real-world scenarios, including ECAC-wide traffic simulations based on operational data, and its implications for supporting proactive, data-driven sector management within an ATFCM context are discussed.

This paper makes the following innovative contributions: (i) it introduces a low-complexity modeling framework to describe the spatiotemporal distribution of aircraft flow within an airspace sector using macroscopic principles; (ii) it derives a nonlinear, normalized power-law formulation governed by an interpretable exponent α, capturing the concentration of traffic near sector exit boundaries and providing a quantitative indicator of clustering intensity; and (iii) it validates the proposed framework using both synthetic and real-world traffic data, showing how the inferred value of α can be used to assess whether sector traffic conditions are suitable for the subsequent deployment of the CAEHO mechanism within an ATFCM decision-support context.

For completeness, Appendix is included at the end of the article and contains glossary tables intended to support the reader.

2. Modeling air traffic flow

This section reviews the main approaches proposed for modeling flight traffic flow, with the aim of identifying a suitable foundation for developing improved methods to represent airspace flows and to support the selection of sectors where the CAEHO mechanism could be applied to ensure its success. A partial differential equation (PDE)-based spatiotemporal model and a nonlinear dwell-time-driven sector eligibility formulation approaches are described to enhance Air Traffic Flow and Capacity Management (ATFCM) with complementary insights into the CAEHO mechanism and its implementation within sector-based traffic management.

2.1. State of the art in modeling flight traffic

Throughout the past decades, various flight traffic models have been developed, each with differing objectives and focus areas [29]. Many academic contributions have concentrated on tactical-level trajectory optimization, conflict detection, and aircraft safety [30–33]. However, these methods often lack macroscopic representations of traffic flow essential for ATFCM tasks such as the capacity-on-demand CAEHO.

In contrast, Eulerian modeling approaches have proven well-suited to ATFCM applications [34,35]. These models describe traffic dynamics over fixed spatial areas (control volumes) and enable analysis of aircraft density, flow rates, and sector occupancy over time. Notable examples, such as [36], model inter-sector aircraft movement through linear PDEs analogous to the Lighthill–Whitham–Richards (LWR) model [37].

2.2. PDE-based air traffic flow model

Needless to say that airspace is inherently three-dimensional, but several authors have explored the idea that flight trajectories can be clustered into flows [38–40]. Thus, sector traffic can be represented as a set of unidimensional flows. Here the model adopts a one-dimensional spatial variable x, representing the remaining distance to the sector boundary along the aircraft's planned trajectory. As a result, the longitudinal progression along the route could be defined capturing the dominant component of aircraft movement relevant to sector occupancy count and remaining dwell time, which are the primary variables driving Clusterized Aircraft Early Handover (CAEHO) decisions. This reduction abstracts away detailed lateral and vertical routing geometry; however, its impact on eligibility estimation is limited because eligibility is driven primarily by remaining dwell time to the sector exit, through which the influence of routing geometry is reflected via its effect on aircraft persistence within the sector, rather than by the explicit geometric complexity of the routes, even in sectors with multiple intersecting flows. Modeling sector flows to one dimension thus significantly improves tractability while retaining the essential dynamics governing flow and eligibility.

This abstraction is further supported by the fact that, consistent with the operational scope defined in Section 1, CAEHO eligibility is restricted to en-route flights operating in cruise conditions, where climbing or descending trajectories are not dominant. Under these conditions, aircraft operate at approximately constant flight levels and speeds, and speed variations remain small relative to the remaining dwell time within a sector. As shown in the flight mechanics and trajectory optimization literature, cruise segments are commonly modeled using constant-altitude, quasi-steady speed assumptions, since residual speed fluctuations have a second-order impact on macroscopic flow measures such as occupancy and dwell time [41,42]. Consequently, the one-dimensional flow representation improves analytical tractability while preserving the dominant dynamics relevant to CAEHO eligibility assessment.

Under this one-dimensional representation, the longitudinal coordinate is considered over the interval $x \in [0, L]$, where $L > 0$ denotes the sector extent along the selected flow-aligned coordinate. The exit boundary corresponds to $x = 0$, while the upstream (entry) boundary corresponds to $x = L$.

In this context, the evolution of aircraft density within a sector is modeled by a one-dimensional conservation law reflecting mass conservation under longitudinal transport [34,43]:

$$\frac{\partial \rho(t,x)}{\partial t} + \frac{\partial}{\partial x}\big(v(x)\rho(t,x)\big) = 0. \tag{1}$$

Here, $\rho(t, x)$ denotes the aircraft density at time t and position $x \in [0, L]$, and $v(x)$ is the signed longitudinal velocity field along the one-dimensional coordinate x.

Eq. (1) is complemented by an initial density distribution and by an inflow condition at the upstream boundary $x = L$; no boundary condition is imposed at the exit boundary $x = 0$, which acts as an outflow boundary.

This density field $\rho(t, x)$, evolving according to Eq. (1), serves as the foundation for estimating the proportion of aircraft eligible for CAEHO. To evaluate eligibility, the *remaining dwell time* $\tau(x)$ is defined as the time required for an aircraft located at position x to reach the exit boundary under uninterrupted motion, associating each longitudinal position x with a corresponding remaining dwell time τ, whose maximum value $T > 0$ corresponds to aircraft located at the upstream boundary $x = L$, such that $\tau \in [0, T]$ with $\tau = 0$ at the exit boundary:

$$\tau(x) = \int_0^x \frac{1}{v(s)}\, ds. \tag{2}$$

Given a time control window Δt, an aircraft is considered eligible for early handover if $\tau(x) \leq \Delta t$. This condition is encoded through the activation function:

$$H(x, \Delta t) = \begin{cases} 1, & \tau(x) \leq \Delta t, \\ 0, & \text{otherwise.} \end{cases} \tag{3}$$

The proportion of aircraft in a flow eligible for early handover at time t is then computed as

$$E(t, \Delta t) = \frac{\displaystyle\int_0^L H(x, \Delta t)\, \rho(t, x)\, dx}{\displaystyle\int_0^L \rho(t, x)\, dx}. \tag{4}$$

This expression quantifies the fraction of traffic satisfying the eligibility condition at a given time. The eligibility function depends on the aircraft distribution $\rho(t, x)$, governed by the continuity equation, and on the velocity profile through the dwell-time mapping. The model remains purely Eulerian, with H acting as a filter on the density field rather than as a dynamic term in the PDE.

2.3. Nonlinear modeling of eligibility

Nonlinear behavior is a well-established characteristic of macroscopic transport and traffic-flow models, where linear representations are known to be insufficient to capture phenomena such as congestion buildup, clustering, and regime transitions. While early kinematic wave formulations introduced nonlinear conservation laws as a baseline representation of traffic dynamics [44,45], subsequent developments have shown that higher-order, non-equilibrium, and decision-influenced dynamics require explicitly nonlinear formulations [46–48].

More recent mathematical work has further emphasized the role of nonlinearity in transport systems subject to boundary interactions, nonlocal effects, and network couplings, where flow feasibility and redistribution cannot be described through linear superposition [49,50]. These studies highlight that nonlinear terms often arise naturally when capacity constraints, coupling conditions, or aggregate decision effects are introduced.

To overcome these limitations, the eligibility formulation is extended from the PDE framework toward a nonlinear cumulative model defined in dwell-time coordinates. For a given CAEHO time window length $\Delta t \in [0, T]$, the cumulative eligibility function $E(\Delta t) \in [0, 1]$ then describes how the proportion of aircraft with remaining dwell time $\tau \leq \Delta t$ grows as the window expands inward from the sector exit boundary. Unlike the PDE-based transport model, this formulation introduces no additional temporal dynamics and captures spatial clustering of eligibility through a nonlinear representation defined directly in dwell-time space.

At this stage, no temporal evolution is implied. The remaining dwell-time variable τ acts solely as an ordering coordinate, and the differential relation introduced in Eq. (5) is used as a constructive mechanism to generate a family of admissible density shapes, rather than as a time-evolution equation.

This approach aligns with recent research employing generalized prediction techniques grounded in the Bernoulli ODE framework [51], and clarifies the transition from PDE-based linear models to fully nonlinear eligibility characterizations proposed in [52].

The classical Bernoulli differential equation can be written as [51]:

$$\frac{dy}{dt} + p(t)\,y = q(t)\,y^{\beta}, \tag{5}$$

where $p(t)$ and $q(t)$ are known functions and $\beta \neq 0, 1$.

Motivated by this formulation, a nonnegative shape function $\theta(\tau)$ is introduced to describe the distribution of traffic along the remaining dwell-time coordinate, and a parsimonious Bernoulli-type relation is adopted as a constructive mechanism to generate a flexible power-law family:

$$\frac{d\theta}{d\tau} = k\,\theta^{\beta}, \tag{6}$$

where:

- $k > 0$ is a scaling parameter,
- β is a nonlinear shape parameter.

Unlike classical time-evolving systems, there is no temporal dynamics in the usual sense; $\theta(\tau)$ represents a snapshot of the density shape over space. The absence of a linear decay term is justified: there is no loss or inflow during the eligibility sweep.

Assuming $\theta(\tau) > 0$ for $\tau > 0$, separation of variables gives:

$$\frac{d\theta}{\theta^{\beta}} = k\,d\tau. \tag{7}$$

For $\beta \neq 1$, integrating both sides yields:

$$\frac{\theta^{1-\beta}}{1-\beta} = k\tau + C. \tag{8}$$

To obtain a physically meaningful shape function, the nonnegative solution that vanishes at the sector exit, corresponding to zero remaining dwell time, is selected. This requirement eliminates the integration constant, yielding:

$$\theta(\tau) = [(1-\beta)k\tau]^{\frac{1}{1-\beta}}, \qquad \tau > 0. \tag{9}$$

Proposition 2.1. *Assume $k > 0$ and $\beta < 1$. Then the function defined in Eq. (9) is nonnegative and satisfies the Bernoulli-type relation, Equation (6), for all $\tau > 0$. Moreover, it vanishes at the sector exit, corresponding to zero remaining dwell time.*

Power-law approximation

The growing mathematical complexity of non-linearities in Eq. (9) to describe potential candidates is worsened by the inherent difficulty of uncertainties in the parameters. There are several approaches to simplify the original equation for a better understanding while preserving key characteristics of he system behavior. For instance, in [53], nonlinear logistic models are used to describe stochastic processes such as biological invasion or wildfire propagation, where model parameters are assumed to exhibit a finite degree of randomness and uncertainty.

It is worth noting that symbolic computation has been employed in related works such as [54] to reformulate nonlinear models exhibiting singular parameter dependencies in closed-form solutions such as Eq. (9). However, in this paper such an approach is not adopted, as parameter uncertainty would still impact the resulting density shape over space, as it can be observed in Eqs. (12). Furthermore, inspired by the work of [55], where the notion of a kernel is introduced as an elementary operator governing the local dynamics of a process (e.g. a reproduction kernel), the Power-Law Approximation is interpreted here as a kernel capturing the fundamental nonlinear growth mechanism underlying Equation (9). This formulation preserves the expected behavior of the original model while reducing sensitivity to parameter uncertainties.

For completeness, it is noted that the transition from Eq. (9) to the power-law expression, Eq. (10), can be verified by symbolic computation through standard algebraic rewrite rules and parameter redefinitions, as documented in the symbolic computation literature [56], confirming that the power-law form is an exact rescaled representation of the same analytical solution.

$$\theta(\tau) = \left(\frac{\tau}{T}\right)^{\alpha}, \tag{10}$$

where:

- α is a shape parameter controlling how aircraft are distributed.

This power-law expression defines a dimensionless shape function that uses a dwell time ratio to describe the relative variation in the aircraft distribution along the remaining dwell time axis. It expresses the tendency of aircraft to cluster near the sector exit or deeper inside, but it does not itself constitute a fully normalized probability density function until divided by its integral.

Parameter correspondence with Bernoulli equation solution

The Bernoulli-based and power-law forms are related by:

$$\theta(\tau) = \left[(1-\beta)k\tau\right]^{\frac{1}{1-\beta}} \quad \longleftrightarrow \quad \left(\frac{\tau}{T}\right)^{\alpha}, \tag{11}$$

which yields the parameter relations:

$$\alpha = \frac{1}{1-\beta}, \quad k = \frac{1}{(1-\beta)T}. \tag{12}$$

Proposition 2.2. *Under the parameter relations (12), the Bernoulli-type solution (9) and the power-law form (10) coincide on $\tau \in [0, T]$.*

Eligibility fraction

The eligibility fraction represents the cumulative proportion of aircraft within the sector that can be selected for early handover when the CAEHO mechanism is applied over a time window of length Δt. Mathematically, this fraction is defined by integrating the shape function $\theta(\tau)$ from the sector exit inward, up to the chosen time window, and normalizing it over the entire dwell time domain (Proposition 2.3).

Proposition 2.3. *Assume Equation (10) holds with $\alpha > -1$ and $T > 0$. Then, for any $\Delta t \in [0, T]$,*

$$E(\Delta t) = \frac{\int_0^{\Delta t} \theta(\tau)\, d\tau}{\int_0^{T} \theta(\tau)\, d\tau} = \left(\frac{\Delta t}{T}\right)^{\alpha+1}. \tag{13}$$

This expression shows that the proportion of aircraft eligible for early handover grows nonlinearly with the size of the CAEHO window Δt, depending on how the dwell times are clustered within the sector. A more clustered distribution near the exit (typically corresponding to $\alpha < 0$) results in higher eligibility for shorter windows, whereas aircraft clustered deeper inside ($\alpha > 0$) require a longer window to reach a comparable proportion. For this formulation to be valid, the integrability condition $\alpha > -1$ must hold, ensuring that the cumulative eligibility remains finite. There is no strict upper bound in theory, although realistic clustering typically produces moderate positive values of α.

The corresponding shape functions for different α values can be observed in Fig. 5.

Formulae (10) and (13) align with related nonlinear models derived from the Bernoulli-type ordinary differential equation framework [51,52], providing an explicit analytical bridge between simple PDE-based occupancy models and realistic clustering assumptions.

3. Causal simulation model

Building upon the previous modeling frameworks, this section explores how the eligibility function can be leveraged to assess the feasibility of applying the Clusterized Aircraft Early Handover (CAEHO) mechanism for a given sector and planned traffic. The objective is not to pinpoint which sectors would benefit most, but rather a decision-support tool providing elaborated information to Air Traffic Flow and Capacity Management (ATFCM) whether the early handover mechanism is likely to be deployable under certain traffic characteristics and prevailing uncertainty. In this context, the dispersion of the parameter α can be interpreted as a feasibility index.

Additionally, the approach leverages the fact that sectors with a higher share of eligible aircraft near the boundary are generally better candidates for proactive control transfer. By systematically applying the eligibility model across space and time, the methodology not only provides a feasibility index through the parameter α but also enables the early detection of sectors where CAEHO could deliver the greatest operational benefit. This supports strategic decision-making in collaborative traffic management settings, enhancing the ability to balance capacity and demand dynamically.

According to planned traffic data, the value of α can be reasonably approximated, since it primarily depends on the distribution of aircraft along the sector. Sector-level parameters such as offset, peak load, and dwell time do not define α directly but help adjust and refine this approximation, especially within a two-hour window prior to operations, when these values can be estimated with relatively high reliability. Although the resulting estimate naturally carries some uncertainty due to possible last-minute changes, the main source of variability comes from flights that are still on the ground, while already airborne aircraft contribute little to this effect. To account for this, additional uncertainty can also be intentionally introduced in simulations, producing a realistic dispersion of α values that helps flow managers judge whether the CAEHO mechanism can be robustly and effectively deployed under the expected traffic conditions.

In this context, α acts as a practical proxy for both the expected eligibility profile and the operational feasibility of applying CAEHO in real time. Combined with its associated uncertainty dispersion, it becomes a valuable decision-support indicator for controllers and flow managers when assessing, during the tactical phase, whether CAEHO is likely to succeed or whether an ATC-capacity regulation should instead be issued to maintain safe and balanced sector occupancy.

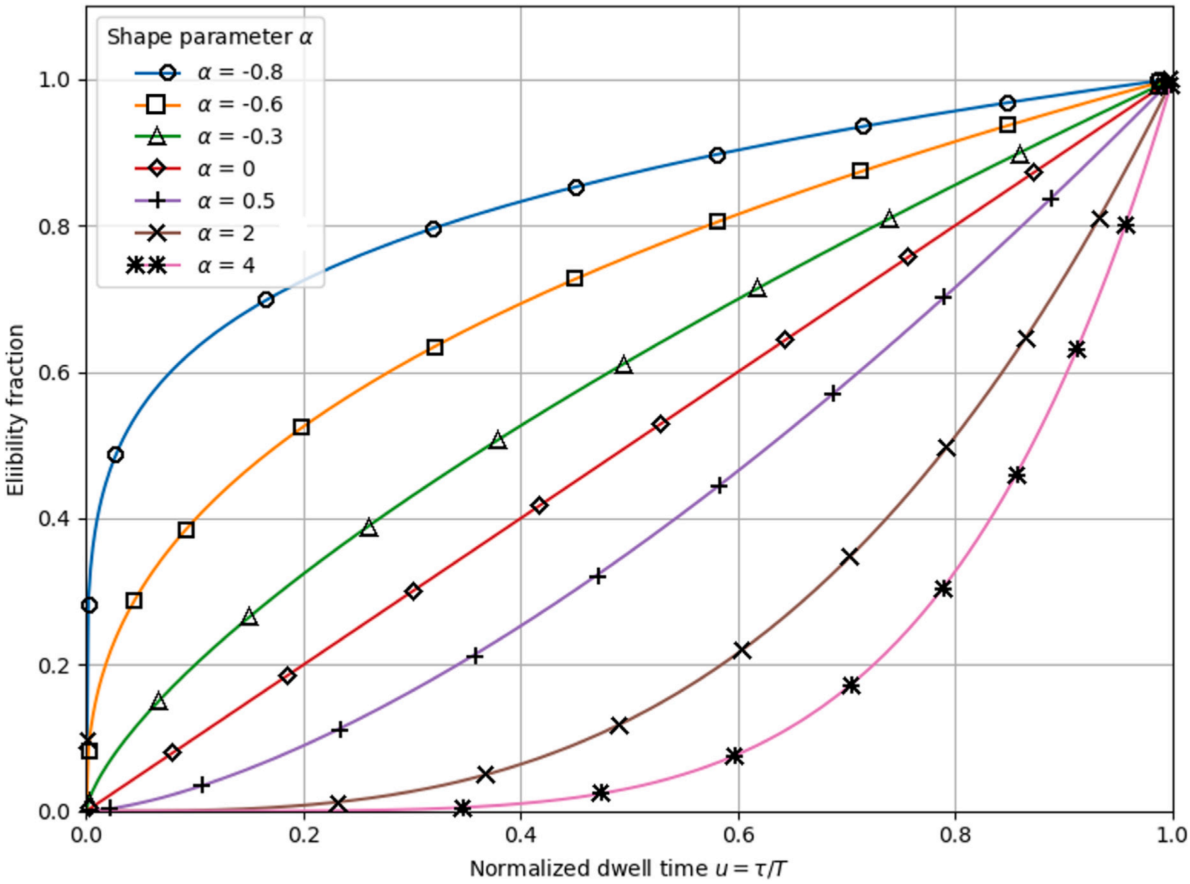

Fig. 5. Normalized eligibility curves for different α values.

3.1. Scenario design

A Discrete Event Simulation (DES) model formalizes the system behavior as a sequence of time-ordered events that cause state changes at stochastic time-stamp intervals. In this study, a DES has been implemented to evaluate different traffic and sector parameter configurations to cross-check simulation results with the proposed theoretical mathematical models.

To provide a practical consistency check, different scenarios have been designed and multi-run simulation results has been analyzed. The main objective is to verify that the theoretical model for the eligibility exponent α consistently reflects the expected relationship between key sector parameters and the resulting CAEHO candidate pool, even in the absence of full operational data.

The scenarios have been designed to model the eligibility shape, which represents how aircraft are distributed relative to the sector exit boundary. This distribution captures whether traffic is balanced toward the exit, concentrated at the entry, or spread more uniformly across the sector. The simulation framework also allows key parameters—such as dwell time, offset level, and peak level—to be adjusted, while introducing controlled uncertainty in entry and exit times and in the peak level itself.

The uncertainty introduced in the simulations is restricted to variability in remaining dwell times and instantaneous occupancy peaks, and is derived from historical discrepancies between planned and flown traffic at the sector level, extracted from AIRAC-based operational datasets (Aeronautical Information Regulation and Control, the standardized cycle used to publish and update aeronautical information [57]). These discrepancies translate directly into fluctuations in entry and exit times and in the number of aircraft present in the sector, without modifying the structural form of the eligibility model.

Under this formulation, uncertainty is not used to quantify the statistical dispersion of the exponent α itself, but to assess the robustness of its qualitative interpretation, namely whether the estimated eligibility pattern remains predominantly exit-clustered, entry-clustered, or near-uniform across realizations.

3.2. Fitting power-law eligibility curves to empirical dwell-time data

It is worth noting that the curves fitted to the raw data have been used to obtain the value of α for each scenario. Accordingly, the discrete-event simulation is executed over n stochastic runs in order to account for uncertainty in the realization of sector traffic.

The resulting eligibility samples are summarized by constructing representative eligibility curves (mean, minimum, and maximum values computed across runs at each fixed Δt). The exponent α is then estimated separately for each of these representative curves, rather than for individual simulation runs.

In this context, a residual for each observation point is defined as:

$$r_i = E_i - \left(\frac{\Delta t_i}{T}\right)^{\alpha+1}, \tag{14}$$

where:

- $i = 1, 2, \ldots, m$ indexes the discrete observation points of the aggregated eligibility curve,
- E_i denotes the empirically observed eligibility value at point i.

The exponent α is estimated by nonlinear least squares through the minimization of the sum of squared residuals:

$$S(\alpha) = \sum_{i=1}^{m} r_i^2, \tag{15}$$

so that the estimated exponent is given by:

$$\hat{\alpha} = \arg\min_{\alpha} S(\alpha). \tag{16}$$

This represents a nonlinear regression problem because the parameter α appears as an exponent, requiring an iterative numerical solution rather than ordinary linear least squares. Various numerical techniques can be applied to estimate α for each curve [58–60].

In this work, the Levenberg–Marquardt method was selected as a well-established and widely used approach for estimating nonlinear exponents [61] (see Algorithm 1). This algorithm follows the standard Levenberg–Marquardt procedure for nonlinear least-squares fitting. Starting from an initial guess, the exponent α is iteratively updated using a damped normal-equations step based on the residual vector and its Jacobian.

Algorithm 1 Levenberg–Marquardt (LM) Estimation of the Nonlinear Exponent α

Require: Observed eligibility values E_i, CAEHO window lengths Δt_i, total dwell time T, initial guess $\alpha^{(0)}$, initial damping factor $\lambda > 0$, convergence tolerance ϵ

Ensure: Estimated exponent $\hat{\alpha}$

Initialize iteration counter $k \leftarrow 0$
Set $\alpha^{(0)}$ and λ
repeat
  for $i = 1$ to m **do**
    Compute residual: $r_i^{(k)} = E_i - \left(\frac{\Delta t_i}{T}\right)^{\alpha^{(k)}+1}$
    Compute Jacobian: $J_i^{(k)} = -\ln\left(\frac{\Delta t_i}{T}\right) \cdot \left(\frac{\Delta t_i}{T}\right)^{\alpha^{(k)}+1}$
  end for
  Form J and r vectors
  Compute LM update: $\delta\alpha = -\left(J^T J + \lambda I\right)^{-1} J^T r$
  Update estimate: $\alpha^{(k+1)} = \alpha^{(k)} + \delta\alpha$
  if $S(\alpha^{(k+1)}) < S(\alpha^{(k)})$ **then**
    Decrease damping: $\lambda \leftarrow \lambda/10$
  else
    Increase damping: $\lambda \leftarrow \lambda \times 10$
  end if
  $k \leftarrow k + 1$
until $|\delta\alpha| < \epsilon$
return $\hat{\alpha} = \alpha^{(k)}$

In summary, Algorithm 1 applies the Levenberg–Marquardt method to iteratively adjust the exponent α so that the modeled eligibility curve matches the aggregated eligibility data.

It is important to distinguish between two different iterative processes in the proposed framework. The number of simulation runs n controls the stochastic sampling of sector traffic and is introduced to stabilize the estimated eligibility shape under uncertainty. In contrast, the nonlinear estimation of the exponent α is performed on a fixed, aggregated eligibility curve and converges in a small number of iterations determined by the numerical tolerance of the Levenberg–Marquardt algorithm.

Accordingly, the choice of n is not driven by the convergence properties of the fitting algorithm, but by the empirical stabilization of the eligibility curves (mean, minimum, and maximum) obtained from the simulations. Once these curves exhibit negligible variation under further increases of n, additional simulation runs provide no meaningful benefit for the subsequent estimation of α.

After aggregation, the eligibility curves are evaluated on a fixed grid of m CAEHO window values Δt_i, which constitute the input data for the nonlinear regression.

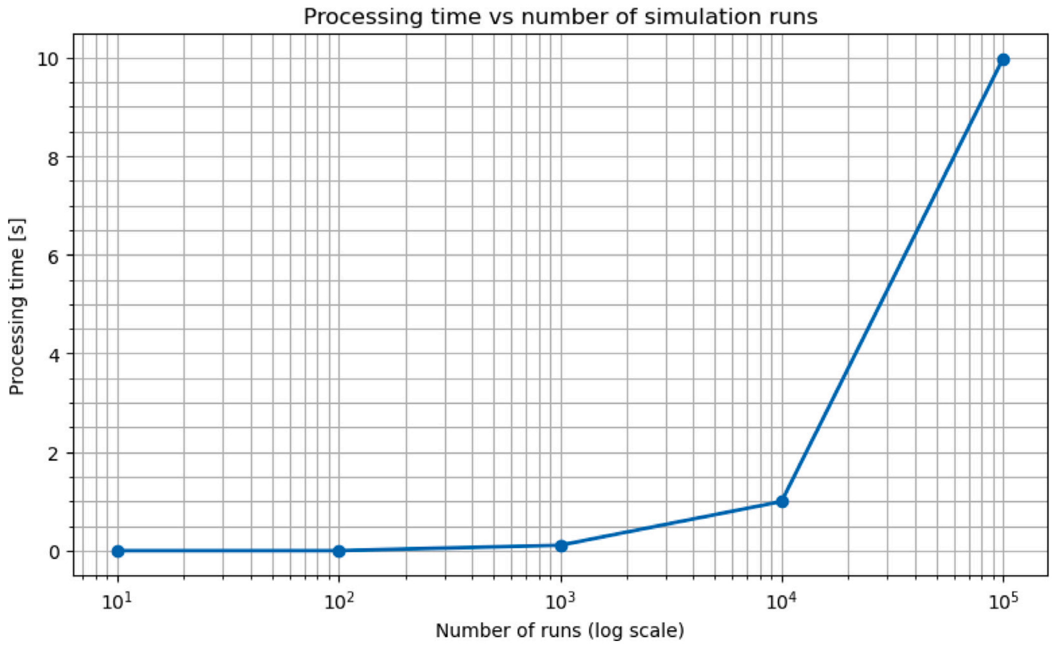

Fig. 6. Wall-clock processing time required to complete one full CAEHO feasibility evaluation cycle as a function of the number of simulation runs.

The computational cost of the proposed approach was evaluated using a synthetic sector-level scenario designed solely for benchmarking purposes. Wall-clock time was measured as a function of the number of simulation runs used to complete one full CAEHO feasibility evaluation cycle.

Here, a full feasibility evaluation cycle comprises the execution of n stochastic simulation runs, the aggregation of eligibility data into representative curves (mean, minimum, and maximum), and the nonlinear estimation of the exponent α from these aggregated curves.

In the scenarios analyzed in this work, values of n on the order of 10^2 simulation runs were found empirically to be sufficient to stabilize the aggregated eligibility curves (mean, minimum, and maximum) within the resolution required for qualitative CAEHO feasibility assessment under stochastic traffic uncertainty. Increasing n beyond this order of magnitude did not materially affect the shape or ordering of these aggregated curves, while incurring additional computational cost; in practice, the complete aggregation over 10^2 simulation runs requires approximately 0.08 s.

The estimation of the exponent α is performed on the representative eligibility curves (mean, minimum, and maximum) constructed from the simulation outputs and does not constitute a significant computational burden. Its numerical cost is negligible compared to the simulation phase and is largely insensitive to the choice of n, since no per-run parameter estimation is carried out.

Fig. 6 reports the processing time for sample sizes ranging from 10 to 10^5 runs.

Overall, these results indicate that the proposed approach is computationally lightweight and compatible with the requirements of tactical decision-support applications when applied selectively to relevant sectors.

3.3. Simulation outcomes

Each simulation is executed 100 times to ensure robust statistical variability. As a result, two types of plots are produced for each simulation. Figs. 7(a) and 8(a) show the eligibility curves obtained from the simulations. The orange curve represents the mean result across the n simulation runs, while the blue curve depicts the maximum threshold observed and the green curve shows the minimum threshold curve obtained from the same set of simulations. The dots represent the raw data points generated by the simulations; superimposed on these, continuous lines display the fitted curves, with the corresponding α values indicated to describe the shape of each fitted distribution.

Figs. 7(b) and 8(b) show individual eligibility curves from a representative subset of the stochastic simulation runs. These panels illustrate the run-to-run variability of the eligibility shape, while the aggregated mean, minimum, and maximum curves reported in Figs. 7(a) and 8(a) are computed using the full set of simulation runs.

The simulation scenarios presented in this section are synthetic and are designed to reproduce representative dwell-time–based traffic distributions within a sector, with aircraft deliberately concentrated either near the exit (Fig. 7) or near the entry (Fig. 8) boundary. These scenarios are used to analyze the behavior of the proposed model and the resulting α values under controlled conditions, while validation against real operational data is addressed later in Section 5.

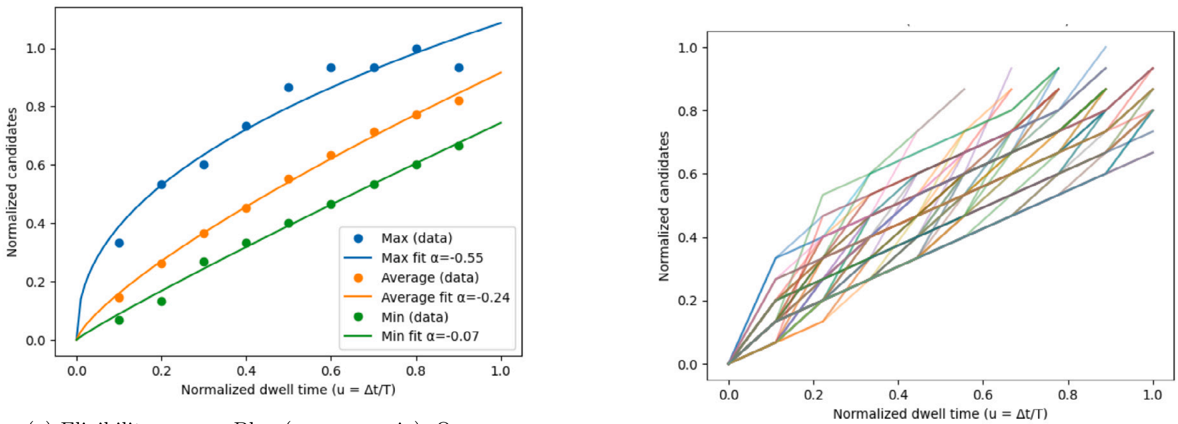

(a) Eligibility curves. Blue (max scenario), Orange (mean scenario), Green (min scenario).

(b) Simulation curves. Individual plots

Fig. 7. Simulated eligibility curves illustrating the distribution of clustered aircraft near the sector exit point.

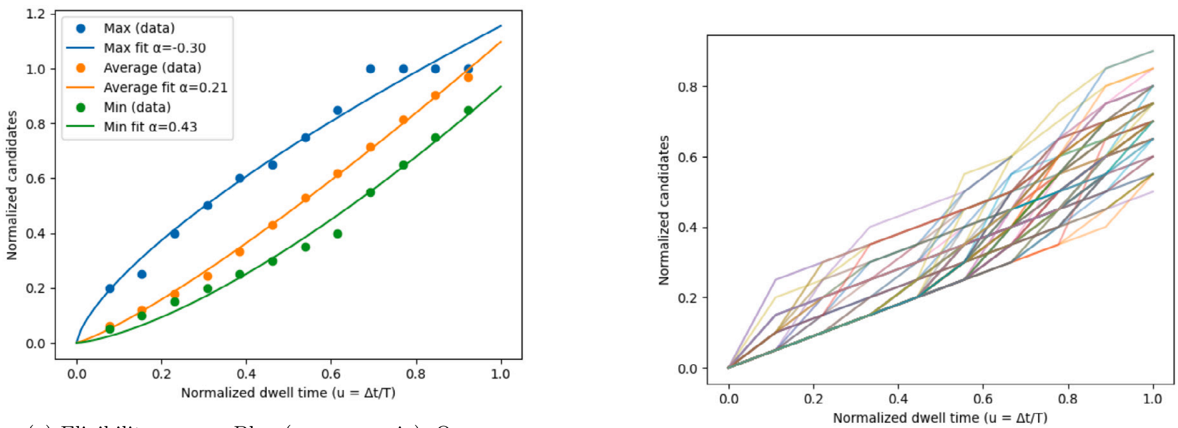

(a) Eligibility curves. Blue (max scenario), Orange (mean scenario), Green (min scenario).

(b) Simulation curves. Individual plots

Fig. 8. Simulated eligibility curves illustrating the distribution of clustered aircraft near the sector entry point.

Proposition 3.1. *Assume the fitted eligibility curves are represented by the power-law model $E(\Delta t) = \left(\frac{\Delta t}{T}\right)^{\alpha+1}$ for $\Delta t \in [0, T]$ with $\alpha > -1$. Then the fitted curve is concave on $(0, T)$ if and only if $-1 < \alpha < 0$, it is linear if and only if $\alpha = 0$, and it is convex on $(0, T)$ if and only if $\alpha > 0$.*

It can be observed from Fig. 7(a) that the curves exhibit negative α values and a concave shape for both the mean and maximum scenarios, while the green curve shows an α value close to zero, resulting in an almost linear behavior. This simulation indicates an aircraft distribution concentrated near the sector exit point, making this sector an excellent candidate for the successful deployment of the CAEHO mechanism. Furthermore, Fig. 7(b) shows the concave behavior of most individual simulation results, confirming the favorable characteristics for implementing CAEHO in this scenario.

On the other hand, Fig. 8 illustrates the opposite scenario, where the aircraft distribution is clustered near the entry point of the sector. This increases the risk of insufficient eligible candidates if the CAEHO mechanism is deployed. This does not imply that CAEHO cannot be applied, but it suggests that, given the inherent uncertainty, there is a higher risk of not finding enough candidates to prevent the need for an ATC-capacity regulation. In Fig. 8(a), both the minimum and mean scenarios display less favorable conditions (with already positive α values), while the maximum scenario still indicates some potential for successful deployment. However, when comparing this with Fig. 8(b), it is evident that the overall tendency is toward a convex behavior, which is generally less favorable for CAEHO implementation.

Taken together, these synthetic scenarios demonstrate the applicability of the proposed ODE-based mathematical model to realistically depict the distribution of aircraft across sectors. The resulting α values provide a practical indicator of eligibility conditions: $\alpha < 0$ reflects traffic distributions that are more favorable to CAEHO deployment, while $\alpha > 0$ indicates progressively less favorable distributions in which early handover opportunities are more limited.

Worthwhile to note that a positive value of α does not imply that CAEHO is infeasible. Instead, it signals that feasibility becomes increasingly conditional on additional operational factors not captured by the distribution shape alone, most notably the severity of the overload relative to sector capacity.

In this sense, the model is not intended to provide a binary feasibility verdict, but rather to act as a decision-support indicator that contextualizes early handover opportunities as a function of traffic distribution shape, to be interpreted jointly with overload magnitude and other operational constraints.

4. Alpha as a CAEHO feasibility index

When sector overload is foreseen, local Flow Management Positions coordinate with the Network Manager (NM) tactical team to assess possible measures, define key parameters, and, if necessary, issue an ATC-capacity regulation at least 2 h before the expected peak occupancy count while some aircraft are still at the airport. The NM then activates and monitors the regulation and informs Aircraft Operators (AOs) through official channels [62]. In this context, the proposed modeling tool offers a practical way to support this decision-making by indicating whether the CAEHO mechanism could be applied instead of a regulation, based on the estimated feasibility index α.

Proposition 4.1. *Let α be the exponent of the eligibility function $E(\Delta t) = \left(\frac{\Delta t}{T}\right)^{\alpha+1}$. Then α provides a qualitative feasibility classification for CAEHO deployment: $\alpha < 0$ indicates a favorable eligibility configuration dominated by aircraft clustered near the sector exit, $\alpha = 0$ corresponds to a neutral configuration, and $\alpha > 0$ indicates a less favorable configuration dominated by aircraft clustered near the sector entry.*

The feasibility of deploying the CAEHO mechanism ultimately depends on how reliably α can be approximated and how its possible dispersion under operational uncertainty is managed. Although α is fundamentally shaped by the distribution of traffic along the sector, parameters such as offset, dwell time, and peak load help adjust its expected value in practice. A wide dispersion means that an expected favorable α could shift under uncertainty, making the mechanism less reliable—or, conversely, opening up opportunities where it may unexpectedly be feasible. Understanding this range helps Flow Management Positions decide during the tactical phase whether CAEHO is likely to work as intended or whether an ATC-capacity regulation remains necessary to maintain safe and balanced occupancy levels.

Although the exponent α is central to the shape of the feasibility index, it should not be interpreted as a standalone decision threshold. Rather, α acts as a contextual indicator describing how eligibility mass is distributed along the remaining dwell-time axis.

Negative values of α indicate that eligible aircraft are predominantly clustered near the sector exit, corresponding to aircraft that are close to handover and therefore more amenable to early delegation with limited coordination risk. Positive values of α reflect eligibility concentrated near the sector entry, where aircraft have longer remaining dwell times and early delegation becomes operationally fragile. Values of α close to zero correspond to a near-uniform eligibility distribution, for which feasibility depends strongly on additional operational factors.

Importantly, no universal thresholds defining "high", "medium", or "low" feasibility can be associated with α alone. The operational meaning of a given α value depends on the surrounding environment, including (i) the severity of the overload, expressed by the number of aircraft that must be delegated and the associated risk tolerance, (ii) the temporal extent of the overload, which may increase uncertainty, (iii) the baseline occupancy level (offset) of the sector, which determines how much residual capacity margin is available before exceedance occurs, and (iv) the structure of feasible delegation options enabled by the traffic geometry and sector adjacency, which may admit either a single viable cluster transfer or, in more favorable configurations, multiple simultaneous delegation options to different adjacent sectors. Accordingly, larger exceedance peaks do not alter the estimated spatial distribution of eligible traffic encoded by α, but they increase the number of aircraft that must be transferred, thereby tightening operational risk constraints on the delegation decision, as discussed in detail in this Section.

As overload severity increases and a larger number of aircraft must be delegated, operational risk tolerance decreases, and feasibility assessments tend to require increasingly negative values of α to ensure sufficient confidence. Conversely, in mild overload situations or when multiple adjacent sectors are available, near-neutral values of α may still support viable CAEHO actions. In this sense, α should be interpreted as a decision-support signal whose relevance emerges only when combined with contextual demand and capacity indicators.

In this context, new scenarios have been simulated to analyze the sensitivity of α dispersion to different sector parameters. Offset levels have been varied from 14 to 4 aircraft and combined with dwell times of 900, 600, and 450 s. Two different traffic patterns have been simulated: the first with traffic density concentrated near the sector exit waypoints, and the second with density concentrated near the entry waypoints. For each combination of dwell time and offset, a Kernel Density Estimate (KDE) [63,64] has been computed to illustrate the resulting α distribution, although only the KDEs for an offset equal to 14 are shown here for clarity. In addition, boxplots are included to help interpret the dispersion and spread of the results.

Fig. 9(a) shows the KDEs of α for the three selected dwell times, illustrating how the curves are clearly shifted toward negative α values (mean values around −0.25 for all cases). This indicates a scenario where the traffic distribution is concentrated near the exit waypoints. Fig. 9(b) presents the same information using boxplots, which help support decision-making by showing the dispersion and spread more clearly. In this case, α values are mostly negative, although in some instances the fitted curve may still produce positive values. Overall, this would generally be considered a favorable case for applying the CAEHO mechanism.

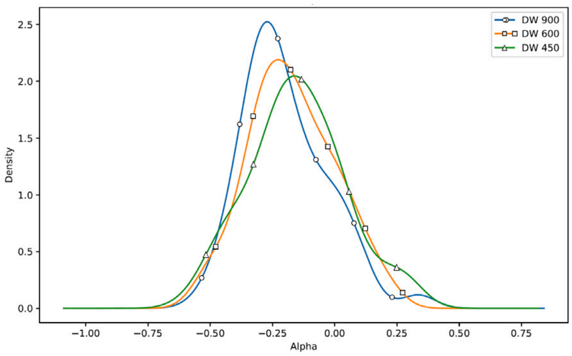

(a) KDEs for dwell time of 450, 600, and 900 seconds. Offset = 14

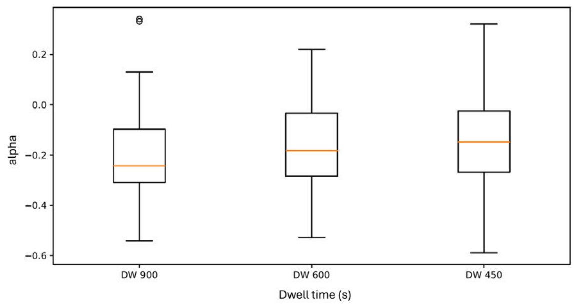

(b) Boxplot of simulated α values for dwell time of 450, 600, and 900 seconds. Offset = 14

Fig. 9. α dispersion for the scenario with traffic near the exit waypoints.

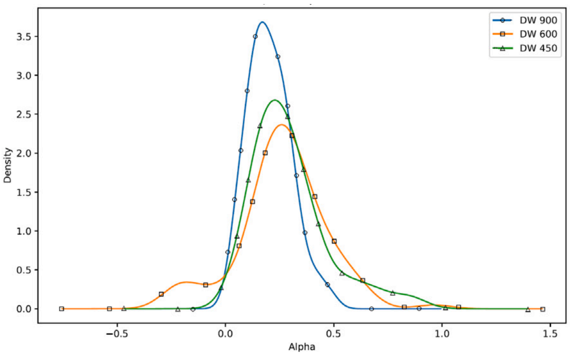

(a) KDEs for dwell time of 450, 600, and 900 seconds. Offset = 14

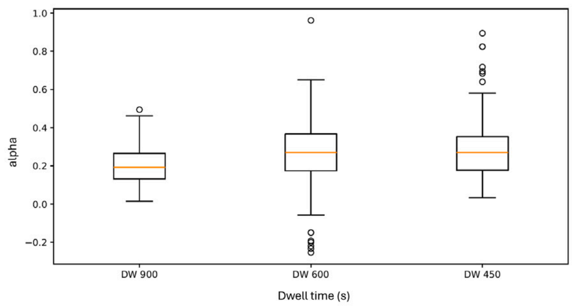

(b) Boxplot of simulated α values for dwell time of 450, 600, and 900 seconds. Offset = 14

Fig. 10. α dispersion for the scenario with traffic near the entry waypoints.

Fig. 10(a) shows the KDEs of α, illustrating how the curves are clearly shifted toward positive α values (around 0.2 and 0.25). This indicates a scenario where the traffic distribution is concentrated near the entry waypoints. Fig. 10(b) presents the same information using boxplots. In this case, α values are mostly positive, although in some instances the fitted curve may still produce negative values. Overall, this would generally be considered a less favorable scenario for applying the CAEHO mechanism, although not necessarily ruled out.

Influence of offset and peak

It has been suggested that the offset and peak levels may influence both the magnitude and the dispersion of α. To examine this effect, two sets of simulations have been conducted. In the first experiment, the dwell time is held constant while the offset configuration is varied. Fig. 11 illustrates how different offset levels affect the distribution of α when the dwell time is fixed at 900 seconds. Fig. 11(a) depicts the corresponding Kernel Density Estimate (KDEs) for various offset levels, showing that α values tend to range from approximately -0.4 for high offset levels (14, 12, and 10) to values closer to zero for lower offset levels (8, 6, and 4). Fig. 11(b) confirms this tendency through boxplots. Overall, higher offset values tend to create a scenario more favorable for the implementation of the CAEHO mechanism, whereas lower offset levels produce the opposite effect.

To check the influence of peak level variations, an additional simulation was carried out with the offset fixed at 14 and the dwell time fixed at 900 seconds. Fig. 12 illustrates that variations in the peak level have little or no influence on the value of α or its dispersion. Both Figs. 12(a) and 12(b) show the same tendency, with α values consistently close to -0.2 and no noticeable differences in dispersion among them.

Overall, these scenarios demonstrate that assessing the dispersion of α provides practical guidance for flow managers to judge the likely success of the CAEHO mechanism and to adapt strategies accordingly. Although this indicator does not, by itself, approve or reject the application of CAEHO, it serves as a valuable supporting tool for more informed decision-making. Additionally, it can highlight how specific sector characteristics, such as offset levels, may support the decision-making process.

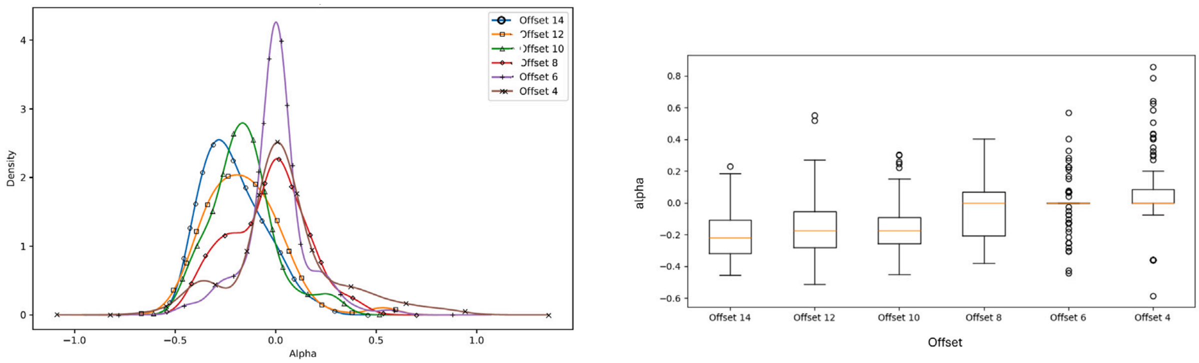

(a) KDEs for offsets 14, 12, 10, 8, 6, 4. Dwell time 900 seconds and peak = 10

(b) Boxplot of simulated α values. Offsets 14, 12, 10, 8, 6, 4. Dwell time 900 seconds and peak = 10

Fig. 11. α dispersion according to offset variation. Fixed dwell time = 900.

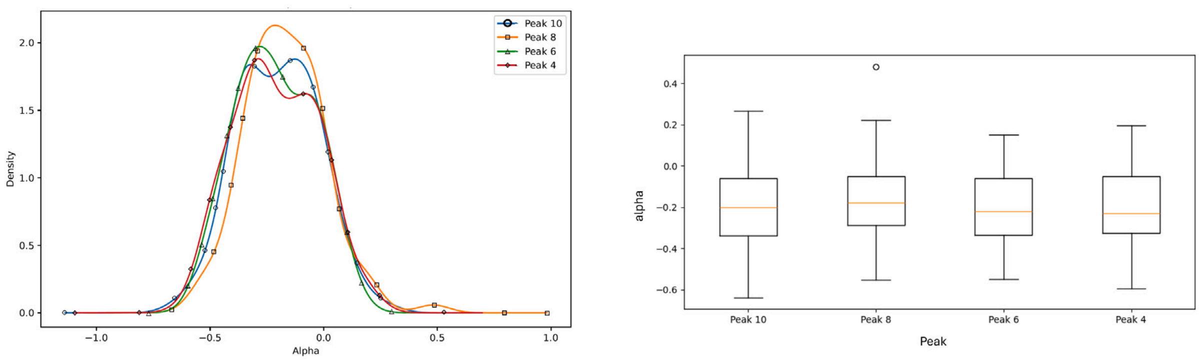

(a) KDEs for peaks 10, 8, 6, 4. Dwell time 900 seconds and offset 14

(b) Boxplot of simulated α values. Peaks 10, 8, 6, 4. Dwell time 900 seconds and offset = 14

Fig. 12. α dispersion according to peak variation. Fixed dwell time = 900 and offset = 14.

5. Experimental validation

To validate the applicability and reliability of the proposed nonlinear model for supporting CAEHO deployment decisions, empirical simulations were carried out. The dataset employed in this study was obtained from AIRAC-based operational data [57], consistently with the data provenance described in Section 3.1.

Using real planned traffic data, the actual positions of each flight were reconstructed along their routes, and their entry and exit times were determined for each sector as needed. Overloaded sectors were identified, and the peaks causing the overload, along with their corresponding times, were calculated to determine the positions of the aircraft during the most critical moments. Supporting tools were designed and used to visualize the positions of the aircraft and to assist decision-making.

Based on the available data, the 27th of July 2024 was selected as the reference day because it recorded the highest number of regulated aircraft of 2024 and a substantial number of ATC-capacity regulations, affecting 122 sectors. Of these 122 regulated sectors, 87 experienced notable delays and were therefore included in the analysis. Eligibility graphs were carried out, and alpha values were calculated as well.

According to the simulations carried out in this study, the spare capacity of the adjacent overloaded sector was first assessed and found to be sufficient in up to 97% of cases where a peak needed to be mitigated. Therefore, from this point onward, the spare capacity of adjacent sectors is assumed to be available. This assumption is applied conditionally to the subset of situations in which such capacity is identified as available, while the remaining cases fall outside the CAEHO applicability domain considered in this work.

5.1. Use cases

As introduced previously, empirical simulations were carried out to validate the nonlinear model proposed in Section 2. Two sectors are illustrated here, each representing a distinct scenario: (i) a sector with aircraft clustered near the exit waypoints ($-1 < \alpha < 0$); (ii) a sector with aircraft concentrated near the entry waypoints ($\alpha > 0$).

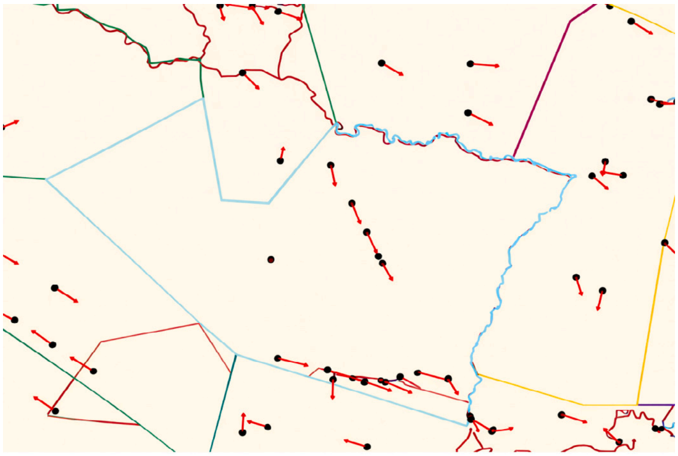

(a) LFEEHE sector physical position of the aircraft

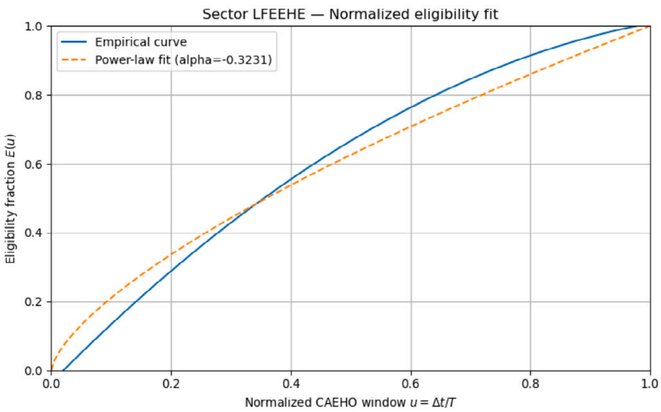

(b) LFEEHE sector eligibility: empirical data plus fitted curve

Fig. 13. LFEEHE sector: spatial distribution and fitted eligibility model.

Validation plots show two different graphs: *(i)* the blue continuous line represents the empirical data; *(ii)* the orange dotted line shows the fitted α curve.

Sector LFEEHE

This sector clearly shows a concentration of aircraft near the exit waypoints, which means that if the power-law form of the nonlinear model is applied, the corresponding value of α should be smaller than 0. Fig. 13(a) depicts the actual positions of the aircrafts in the sector on 27/07/2024 at 06:40:00. As shown in Fig. 13(b), the fitted curve indeed corresponds to an α value smaller than 0, specifically -0.32.

When analyzing the spatio-temporal situation of the aircraft, it is important to consider not only their positions but also their headings, as the heading indicates whether a flight is near the exit waypoints or the entry waypoints.

Sector LQSBHT37

In this case, the sector displays a distribution where most aircraft are concentrated near the entry waypoint and therefore remain far from the exit points. This implies that if the power-law form of the nonlinear model is applied, the resulting α value should be greater than 0. Fig. 14(a) shows the actual flight positions within the sector on 27/07/2024 at 20:06:00. As illustrated in Fig. 14(b), the fitted eligibility curve confirms that the estimated α is indeed greater than 0, specifically 0.92.

Based on this validation, it can be concluded that the power-law form of the nonlinear model, derived from Bernoulli's ODE, provides an accurate representation of the distribution of aircraft within the sectors and supports its practical applicability for assessing CAEHO feasibility in real scenarios.

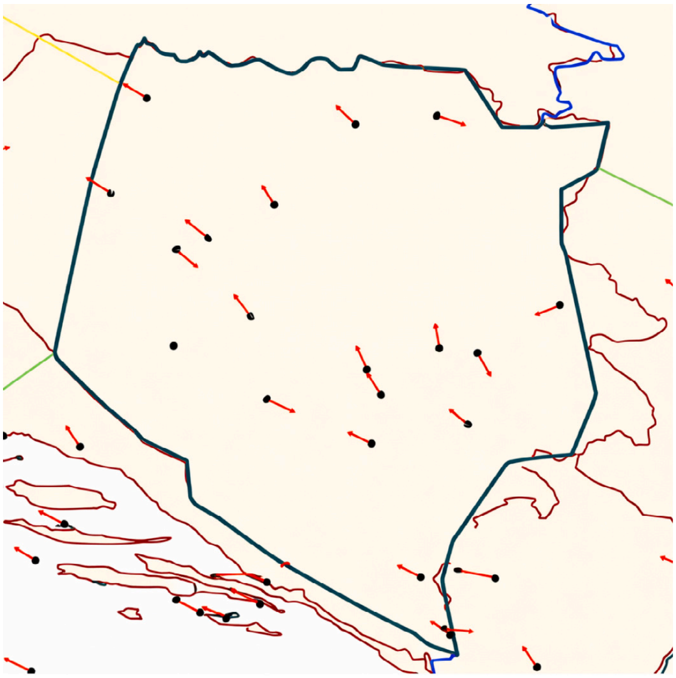

(a) LQSBHT37 sector

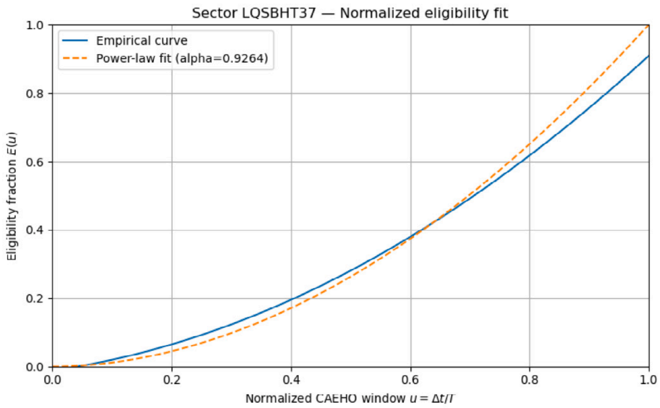

(b) LQSBHT37 sector eligibility: empirical data plus fitted curve

Fig. 14. LQSBHT37 sector: spatial distribution and fitted eligibility model.

6. Operational performance validation

The analytical developments introduced in the previous sections aim to characterize CAEHO eligibility through a compact nonlinear descriptor of traffic geometry within an airspace sector. To illustrate that this formulation constitutes more than a purely theoretical construct, the present section provides a quantitative experimental validation against high-fidelity, Europe-wide traffic simulations. The objective is to assess, using real operational data and explicit numerical evidence, whether the proposed model—and in particular the exponent α derived from remaining dwell time distributions—is able to explain and discriminate CAEHO feasibility outcomes observed in practice during sector overload situations.

6.1. Operational rationale of CAEHO and flow-level delegation

CAEHO is considered here from the perspective of its operational applicability during sector overload peaks. Rather than revisiting the general rationale of early delegation, the focus is placed on how overload exceedance can be mitigated through

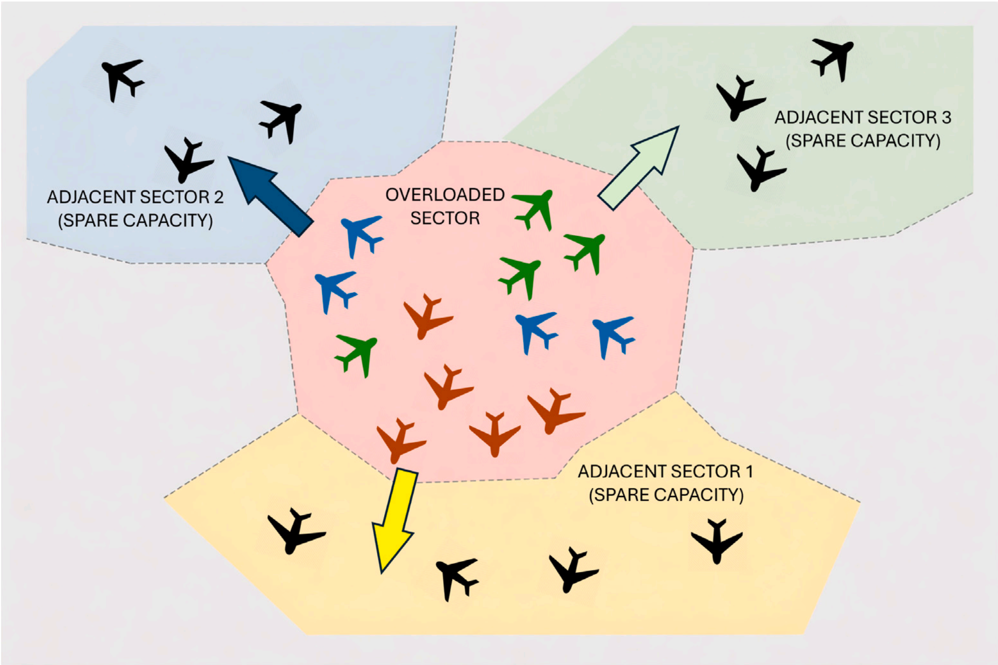

Fig. 15. Schematic illustration of an overloaded sector and its decomposition into outbound flows directed toward adjacent sectors.

the delegation of aircraft toward adjacent sectors, subject to their available downstream capacity. In operational practice, such delegation may involve the transfer of control of one or several clusters of aircraft, potentially distributed across different outbound directions and absorbed by multiple adjacent sectors.

Although previous analyses have shown that, from an aggregate capacity perspective, a large majority of overload peak situations could be resolved provided that sufficient spare capacity exists in one or more adjacent sectors, this sector-level view masks an important operational aspect. At an overload peak, aircraft within a sector are not uniformly distributed, but are organized along a finite set of outbound directions according to their planned trajectories. As a result, delegation opportunities do not arise homogeneously at the sector level, but materialize through a set of outbound flows, each directed toward a specific adjacent sector. Fig. 15 illustrates this directional decomposition.

For instance, an overloaded sector may contain a sufficient total number of aircraft at the overload instant, while these aircraft are unevenly split across several outbound flows. In such cases, the resolution of the overload episode may require the delegation of multiple clusters, possibly along different outbound directions, depending on the residual capacity available in the corresponding adjacent sectors. Consequently, CAEHO feasibility cannot be inferred from the aggregate aircraft count alone, since each adjacent sector must independently possess sufficient capacity to absorb the aircraft associated with the delegated cluster(s).

Although the exponent α is derived from the remaining dwell time distribution within a sector and therefore characterizes the sector-level traffic geometry, its operational relevance necessarily arises through outbound flows. At overload peaks, the sector-level distribution is effectively decomposed into directional components according to aircraft heading and adjacent sectors. Each outbound flow thus represents a directional projection of the same underlying sector geometry. Analyzing flows individually complements the sector-level nature of α by accounting for the fact that CAEHO actions are constrained by adjacent-sector capacities and must be implemented along specific outbound directions.

The validation presented in this section therefore focuses on the flow-level manifestation of sector traffic geometry. At each overload peak, flows are identified according to the adjacent sector toward which aircraft are heading, and eligibility is evaluated on the basis of remaining dwell time within a prescribed temporal window. Feasibility is assessed under a conservative condition, by examining whether an individual outbound flow provides a sufficient number of eligible candidates to contribute to the absorption of the overload exceedance. This single-flow assessment does not preclude multi-flow delegation in operational practice; rather, it provides a lower-bound and analytically tractable evaluation of the role played by traffic geometry along individual flows.

6.2. Dataset and experimental scope

The validation is conducted on a full-day traffic dataset corresponding to 27 July, covering the entire European Civil Aviation Conference (ECAC) area (Fig. 16). The dataset is derived from operational AIRAC-based traffic data, and reflects the real traffic demand and sector configurations observed on that day. High-fidelity traffic simulations are subsequently carried out by the authors

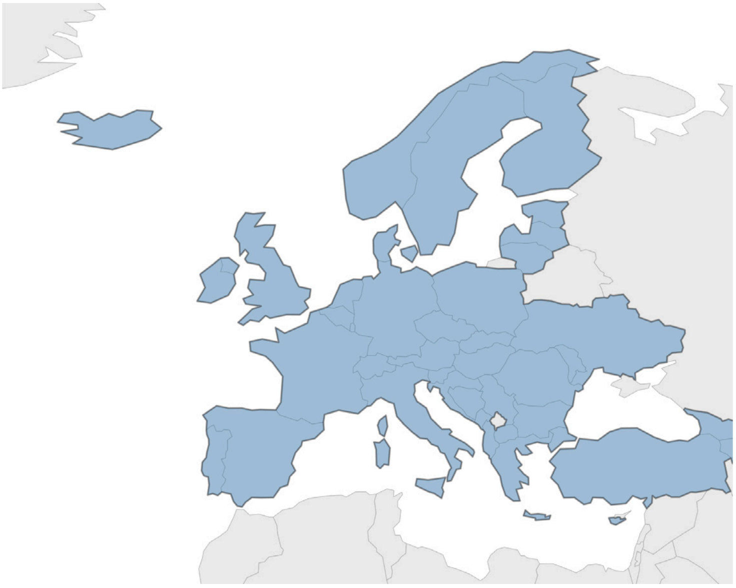

Fig. 16. Geographical scope of the study covering the ECAC area.

using this operational data, with the objective of reproducing realistic sector loads and evaluating the applicability of the CAEHO mechanism under representative operational conditions.

For each en-route sector, the simulation framework identifies overload occurrences, quantifies the corresponding exceedance levels, and evaluates CAEHO feasibility at overload peak instants by explicitly examining aircraft remaining dwell times, headings, and outbound adjacent sectors. Feasibility is determined constructively by verifying whether a sufficient number of aircraft satisfy the CAEHO eligibility criterion within a prescribed temporal window.

Across the analyzed day, 85 en-route sectors exhibit at least one overload episode, yielding a total of 97 distinct overload peak instants. At each overload peak, aircraft are partitioned into outbound flows according to their planned trajectories toward adjacent sectors, resulting in 288 distinct sector-to-sector flows. For each flow, the observed traffic distribution is used to estimate the exponent α, which characterizes the degree of exit concentration inherited from the underlying sector traffic geometry and is compared against CAEHO feasibility outcomes produced by the simulation.

6.3. Flow-level estimation of α

For each outbound flow associated with an overloaded sector, the exponent α is estimated at overload peaks using the normalized power-law representation introduced in Eq. (13). Although α originates from a sector-level description of traffic geometry, its estimation at the flow level captures how this geometry is manifested along specific exit directions that are operationally relevant to delegation decisions.

6.4. CAEHO feasibility assessment

CAEHO feasibility is assessed by comparing, for each overload episode and outbound flow, the number of eligible aircraft within a given remaining dwell time window Δt to the minimum number of candidates required to absorb the observed exceedance. Feasibility is therefore evaluated at the flow level, reflecting the operational constraint that a single adjacent sector must be able to accommodate the delegated aircraft associated with that flow.

The analysis is repeated for multiple temporal horizons $\Delta t \in \{240, 300, 360, 420, 480\}$ s in order to evaluate how the explanatory and discriminative power of α evolves with the available temporal margin.

6.5. Flow-level validation outcomes

Table 1 reports the observed flow-level CAEHO feasibility rates, aggregated across all overloaded sectors and overload peak episodes. In this context, feasibility is defined at the level of individual outbound flows and corresponds to the proportion of flows that, when considered in isolation, provide a sufficient number of eligible aircraft within a given remaining dwell time window to contribute to the absorption of an overload peak. These rates do not represent the overall probability of resolving overload situations at the sector level, but rather quantify the capability of individual flows under conservative assessment conditions.

Table 1
Flow-level CAEHO feasibility rates (%) by remaining dwell time window and sign of α.

Remaining dwell time Δt (s)	$\alpha < 0$	$\alpha \geq 0$
240	39.5	21.6
300	46.5	25.7
360	48.1	33.8
420	55.0	40.5
480	57.4	43.2

For short remaining dwell time windows, a clear statistical separation between the two flow classes emerges. At $\Delta t = 240$ s, flows characterized by $\alpha < 0$ exhibit a feasibility rate nearly twice that of flows with $\alpha \geq 0$. This indicates that exit-concentrated traffic configurations are, on average, more likely to provide a sufficient number of eligible aircraft along a given outbound direction under tight temporal constraints.

It is important to emphasize that these flow-level feasibility rates should not be interpreted as the overall success rate of CAEHO in eliminating sector overloads. In operational settings, the resolution of an overload episode may involve the delegation of multiple clusters simultaneously, potentially distributed across several outbound flows and absorbed by multiple adjacent sectors. Such coordinated multi-flow delegation would naturally increase the probability of resolving an overload episode beyond the conservative single-flow assessment reported here.

Accordingly, positive values of α do not imply that CAEHO is infeasible for a given flow, nor do negative values guarantee overload resolution. The sign of α modulates the likelihood that an individual flow can meaningfully contribute to overload absorption, while the actual operational outcome depends on additional factors, according to CAEHO operational framework.

As the remaining dwell time window increases, the observed separation between flow classes progressively diminishes. For $\Delta t \geq 420$ s, feasibility approaches a saturation regime in which most flows provide eligible candidates independently of their geometric structure. In this regime, candidate availability is dominated by aircraft count rather than by spatial organization, and the discriminative power of α naturally decreases.

Taken together, these results support the interpretation of α as a flow-level decision-support indicator derived from sector traffic geometry. Its practical value lies in prioritizing outbound flows for potential delegation under limited temporal margins, rather than in predicting overall CAEHO performance at the sector level.

7. Conclusions

This study has introduced a modeling framework for assessing a capacity-on-demand Air Traffic Flow and Capacity Management (ATFCM) mechanism that can avoid unnecessary air traffic ground regulations. A PDE-based spatiotemporal conservation law was presented as a physically consistent foundation to describe the evolution of aircraft density within a sector. However, recognizing that a purely Eulerian approach does not naturally capture the nonlinear clustering patterns that determine handover readiness, its role in this work remains illustrative and supportive. This distinction highlights that early handover feasibility is governed not by average flow evolution alone, but by inherently nonlinear aggregation effects within the traffic distribution.

To address this limitation, a complementary nonlinear eligibility formulation based on a Bernoulli-type ordinary differential equation was developed to model the spatial distribution of eligible aircraft as a function of remaining dwell time. The resulting normalized power-law representation, governed by the exponent α, successfully captures how eligibility accumulates inward from the sector exit boundary. In practical terms, negative α values indicate that aircraft are clustered near the sector exit – an ideal condition for Clusterized Aircraft Early Handover (CAEHO) deployment – while higher α values suggest that traffic remains dispersed, reducing immediate handover potential. This behavior illustrates how small variations in traffic organization can lead to disproportionately different eligibility outcomes, reflecting the fundamentally nonlinear nature of the problem.

Validation through synthetic scenarios and empirical data has confirmed that this Bernoulli-based model realistically represents the clustering behavior of aircraft within a sector and provides an interpretable metric for sector prioritization. Notably, the findings demonstrate that while α could be calculated exactly for planned traffic, is better to consider α dispersion values to tackle air traffic uncertainties. The resulting spread of α values provides insight into the sensitivity of CAEHO feasibility to nonlinear perturbations in traffic distribution, providing a useful qualitative indicator of the likely clustering shape of aircraft and acts as a practical proxy for the risk of deploying CAEHO under certain conditions. Patterns observed in the simulations show how α can offer a useful first step for flow managers and local controllers to identify candidate sectors and decide whether CAEHO might safely replace an ATC-capacity regulation, without the need for complex data processing.

The analytical results are further supported by ECAC-wide experimental validation on realized traffic data, confirming the practical discriminative value of the proposed eligibility descriptor under realistic overload conditions.

In summary, this work shows that the Bernoulli ODE-based nonlinear eligibility model is a practical, robust decision-support tool for assessing early handover feasibility. By explicitly accounting for nonlinear clustering effects, the proposed approach captures behaviors that cannot be inferred from linear or averaged traffic representations alone. By integrating this approach into tactical planning, stakeholders can better balance demand and capacity, maintain safety margins, and reduce costly delays. Future research should extend this framework to dynamic multi-sector applications, incorporate uncertainty metrics (resilience), and refine its integration with operational ATFCM systems to further support proactive, data-driven airspace management.

CRediT authorship contribution statement

Alfons Borràs: Writing – original draft, Validation, Software, Methodology, Investigation, Formal Analysis, Data curation, Conceptualization. **Laura Calvet:** Writing – review & editing. **Miquel Àngel Piera:** Writing – review and editing, Supervision, Software, Project Administration, Funding acquisition, Formal Analysis, Resources. **Gabriella Gigante:** Writing – review & editing, supervision.

Acknowledgments

This work has received funding from the SESAR Joint Undertaking under the European Union Horizon Europe research and innovation programme (Grant Agreement No. 101166947, ANTICIPATE) and from Grant PK620616 PID2023-150782OB-C21, funded by MICIU/AEI/ 10.13039/501100011033.

Appendix. Glossary

See Tables A.2 and A.3.

Table A.2
Glossary of symbols and parameters.

Symbol	Description
t	Time variable in the PDE-based flow model.
x	Spatial coordinate along the sector flow axis ($x = 0$ at sector exit).
L	Length of the sector domain along the modeled flow.
$v(x)$	Aircraft velocity as a function of position.
$\rho(t, x)$	Aircraft density at time t and position x.
$\tau(x)$	Remaining dwell time to the sector exit.
T	Total dwell-time span of the sector.
Δt	CAEHO eligibility time window.
$H(t, x)$	Eligibility indicator function.
$E(t, \Delta t)$	Fraction of aircraft eligible for CAEHO.
$\theta(\tau)$	Eligibility shape function along dwell time.
α	Power-law exponent governing clustering intensity.
β	Nonlinear shape parameter in the Bernoulli ODE.
k	Scaling parameter in the Bernoulli formulation.
r_i	Residual of observation i in curve fitting.
$\hat{\alpha}$	Estimated value of α.
Offset	Baseline sector occupancy level.
Peak	Maximum occupancy above the offset level.

Table A.3
Glossary of acronyms used in the manuscript.

Acronym	Meaning
ACC	Area Control Centre.
ADP	Air Traffic Management Daily Plan.
AIRAC	Aeronautical Information Regulation and Control cycle.
ANSP	Air Navigation Service Provider.
AO	Aircraft Operator.
ATC	Air Traffic Control.
ATCo	Air Traffic Controller.
ATFCM	Air Traffic Flow and Capacity Management.

(continued on next page)

Table A.3 (*continued*).

Acronym	Meaning
ATFM	Air Traffic Flow Management.
CAEHO	Clusterized Aircraft Early Handover.
CASA	Computer Assisted Slot Allocation algorithm.
DAC	Dynamic Airspace Configuration.
DAS	Dynamic Airspace Sectorization.
DES	Discrete Event Simulation.
ECAC	European Civil Aviation Conference.
FCA	Flight-Centric Airspace.
FMP	Flow Management Position.
INAP	Integrated Network Management and ATC Planning phase.
KDE	Kernel Density Estimate.
LM	Levenberg–Marquardt method.
LWR	Lighthill–Whitham–Richards model.
NM	Network Manager (EUROCONTROL).
NOP	Network Operations Plan.
ODE	Ordinary Differential Equation.
PDE	Partial Differential Equation.
SESAR	Single European Sky ATM Research programme.
STAM	Short-Term ATFCM Measures.

References

[1] N. Ahrenhold, I. Gerdes, T. Mühlhausen, A. Temme, Validating dynamic sectorization for air traffic control due to climate sensitive areas: Designing effective air traffic control strategies, Aerospace 10 (5) (2023) 405.
[2] F. Furini, C.A. Persiani, P. Toth, The time dependent traveling salesman planning problem in controlled airspace, Transp. Res. Part B: Methodol. 90 (2016) 38–55.
[3] P. Flener, J. Pearson, Automatic airspace sectorisation: A survey, 2013, arXiv preprint arXiv:1311.0653.
[4] J. Nosedal Sánchez, Aircraft Departure Synchronization to Reduce ATC En-Route Interventions (Ph.D. thesis), Universitat Autònoma de Barcelona, Bellaterra, Spain, 2016.
[5] G.N. Lui, G. Lulli, M.F. Lema-Esposto, R.L. Martinez, Airspace sector design: An optimization approach, SESAR Innov. Days (2024).
[6] T. Treimuth, Dynamic optimization of airspace sector grouping (Ph.D. thesis), Institut National Polytechnique de Toulouse-INPT, Toulouse, France, 2018.
[7] S. Starita, A.K. Strauss, X. Fei, R. Jovanović, N. Ivanov, G. Pavlović, F. Fichert, Air traffic control capacity planning under demand and capacity provision uncertainty, Transp. Sci. 54 (4) (2020) 882–896.
[8] C.-L. Wu, K. Law, Modelling the delay propagation effects of multiple resource connections in an airline network using a Bayesian network model, Transp. Res. Part E: Logist. Transp. Rev. 122 (2019) 62–77.
[9] P. Choroba, L. van der Hoorn, Towards a more harmonised and wider use of short-term ATFCM measures (STAM), in: 30th Congress of the International Council of the Aeronaurical Sciences, 2016, pp. 25–30.
[10] S. Ruiz, H. Kadour, P. Choroba, A novel air traffic flow management model to optimise network delay, in: 13th USA/Europe ATM Seminar, Vienna, 2019.
[11] EUROCONTROL, Data | aviation intelligence portal, 2024, URL https://ansperformance.eu/data/, (Accessed: February 9, 2026).
[12] A. Cook, G. Tanner, S. Cristobal, M. Zanin, Delay propagation–new metrics, new insights, in: Eleventh USA/Europe Air Traffic Management Research and Development Seminar, EUROCONTROL/FAA, 2015.
[13] L. Delgado, G. Gurtner, T. Bolić, L. Castelli, Estimating economic severity of air traffic flow management regulations, Transp. Res. Part C: Emerg. Technol. 125 (2021) 103054.
[14] I. Gerdes, A. Temme, M. Schultz, Dynamic airspace sectorisation for flight-centric operations, Transp. Res. Part C: Emerg. Technol. 95 (2018) 460–480.
[15] SESAR. Joint Undertaking, PJ.09-W2-44 Contextual Note: Enhanced Integration of AU trajectory definition and Network Management processes, 2022, https://www.sesarju.eu/sites/default/files/documents/solution/SolPJ.09-W2-44-V3_Contextual_Note.pdf, (Accessed: February 9, 2026).
[16] EUROCONTROL Performance Review Commission, Performance insight #7: Reorganising ATS with virtual centres, 2023, https://www.eurocontrol.int/publication/performance-insight-7-reorganising-ats-virtual-centres, (Accessed: February 9, 2026).
[17] A.T.M. Halawani, Smart roundabout coordination systems for sustainable urban mobility, Civ. Eng. J. 11 (2) (2025) 623–634, http://dx.doi.org/10.28991/CEJ-2025-011-02-013.
[18] M. Rahman, M.A. Rahim, U. Ayman, A. Sohel, M.A. Hossain, M.A. Moni, A. Moustafa, Real-time vehicle type detection and counting for emission pollution monitoring and traffic violation identification, Emerg. Sci. J. 9 (2) (2025) 959–976.
[19] I. Damyanov, G. Mladenov, D. Saliev, R. Miletiev, K. Dimitrov, V. Hristov, Infrared thermal monitoring of intersection elements of urban road infrastructure and road traffic via drone, Civ. Eng. J. 11 (5) (2025) 1739–1755.
[20] SESAR Joint Undertaking, ANTICIPATE: Advancing air traffic capacity management in Europe, Project portal, SESAR Joint Undertaking, 2024, https://www.sesar.eu/projects/ANTICIPATE. (Accessed: February 9, 2026).
[21] G. Martin, M. Piera, A causal STAM model to increase airspace network capacity, in: Proceedings of the 11th EUROSIM Congress, Amsterdam, The Netherlands, 2023.
[22] SESAR Joint Undertaking and EUROCONTROL, PJ19.04: Performance Framework (2019), Edition 01.00.01, SESAR Joint Undertaking / EUROCONTROL, Brussels, Belgium, 2019, URL https://www.sesarju.eu/sites/default/files/documents/awards2021/SESAR%20Performance%20Framework%20ed_%2001_00_01%20-%202019.pdf, Version 01.00.01, 30 November 2019.

[23] A. Borràs, L. Calvet, M.À. Piera, Increasing airspace capacity by improving ATCo's efficiency through an innovative handover mechanism, Comput. Ind. Eng. 196 (2024) 110513.
[24] A. Borràs, M.À. Piera, G. Acampora, F. Gargiulo, V. Sangermano, B. Blom, R. Weger, Enhancing dynamic airspace configuration and flight-centric ATC through clusterized aircraft early handover, in: Proceedings of the SESAR Innovation Days 2025, Europe, 2025, URL https://www.sesarju.eu/sites/default/files/documents/sid/2025/papers/SIDs_2025_paper_25-final.pdf.
[25] International Civil Aviation Organization, Procedures for Air Navigation Services — Air Traffic Management (PANS-ATM, Doc 4444), 16th ed., International Civil Aviation Organization, 2016.
[26] H.G. Visser, Terminal area traffic management, Prog. Aerosp. Sci. 28 (4) (1991) 323–368.
[27] G.G.N. Sandamali, R. Su, Y. Zhang, Flight routing and scheduling under departure and en route speed uncertainty, IEEE Trans. Intell. Transp. Syst. 21 (5) (2020) 1915–1928, http://dx.doi.org/10.1109/TITS.2019.2907058.
[28] European Civil Aviation Conference (ECAC), Member states — ECAC, 2025, https://www.ecac-ceac.org/about-ecac/member-states/, (Accessed: February 9, 2026).
[29] C. Cummings, H. Mahmassani, Airspace congestion, flow relations, and 4-D fundamental diagrams for advanced urban air mobility, Transp. Res. Part C: Emerg. Technol. 159 (2024) 104467.
[30] Z.-H. Mao, E. Feron, K. Bilimoria, Stability and performance of intersecting aircraft flows under decentralized conflict avoidance rules, IEEE Trans. Intell. Transp. Syst. 2 (2) (2001) 101–109.
[31] Y. Liu, A progressive motion-planning algorithm and traffic flow analysis for high-density 2D traffic, Transp. Sci. 53 (6) (2019) 1501–1525.
[32] M. Ribeiro, J. Ellerbroek, J. Hoekstra, Review of conflict resolution methods for manned and unmanned aviation, Aerospace 7 (6) (2020) 79.
[33] G. Stroe, I.-C. Andrei, Automated conflict resolution in air traffic management, INCAS Bull. 9 (1) (2017) 91–104.
[34] A.M. Bayen, R.L. Raffard, C.J. Tomlin, Adjoint-based control of a new Eulerian network model of air traffic flow, IEEE Trans. Control Syst. Technol. 14 (5) (2006) 804–818.
[35] D.B. Work, A.M. Bayen, Convex formulations of air traffic flow optimization problems, Proc. IEEE 96 (12) (2008) 2096–2112.
[36] P. Menon, G. Sweriduk, T. Lam, G. Diaz, K.D. Bilimoria, Computer-aided Eulerian air traffic flow modeling and predictive control, J. Guid. Control Dyn. 29 (1) (2006) 12–19.
[37] M. Treiber, A. Kesting, M. Treiber, A. Kesting, The Lighthill–Whitham–Richards model, in: Traffic Flow Dynamics: Data, Models and Simulation, Springer, 2013, pp. 81–126.
[38] F.P. Moreno, V.F.G. Comendador, R.D.-A. Jurado, M.Z. Suárez, D. Janisch, R.M.A. Valdés, Methodology of air traffic flow clustering and 3-D prediction of air traffic density in ATC sectors based on machine learning models, Expert Syst. Appl. 223 (2023) 119897.
[39] A. Chandra, S. Hazra, A. Verma, The integration of En route flow optimization, complex network clustering, and rule-based approach to airspace sub-sectorization for enhanced air traffic monitoring, J. the Air Transp. Res. Soc. 3 (2024) 100036.
[40] Y. Chen, Y. Zhao, Y. Wu, Recent progress in air traffic flow management: A review, J. Air Transp. Manag. 116 (2024) 102573.
[41] A. Franco, A. Valenzuela, D. Rivas, Optimal control of cruise flight at constant altitude, in: 27th International Congress of the Aeronautical Sciences, ICAS, 2010.
[42] V.E. Atasoy, C. Cetek, Enhanced cruise range prediction for narrow-body turbofan commercial aircraft based on QAR data, Aeronaut. J. 125 (1286) (2021) 672–701.
[43] A.M. Bayen, R.L. Raffard, C.J. Tomlin, Eulerian network model of air traffic flow in congested areas, in: Proceedings of the 2004 American Control Conference, Vol. 6, IEEE, 2004, pp. 5520–5526.
[44] M.J. Lighthill, G.B. Whitham, On kinematic waves II. A theory of traffic flow on long crowded roads, Proc. R. Soc. Lond. Ser. A. Math. Phys. Sci. 229 (1178) (1955) 317–345.
[45] P.I. Richards, Shock waves on the highway, Oper. Res. 4 (1) (1956) 42–51.
[46] A. Aw, M. Rascle, Resurrection of "second order" models of traffic flow, SIAM J. Appl. Math. 60 (3) (2000) 916–938.
[47] H.M. Zhang, A non-equilibrium traffic model devoid of gas-like behavior, Transp. Res. Part B: Methodol. 36 (3) (2002) 275–290.
[48] D. Helbing, Traffic and related self-driven many-particle systems, Rev. Modern Phys. 73 (4) (2001) 1067.
[49] R.M. Colombo, G. Guerra, Hyperbolic balance laws with a non local source, Comm. Partial Differential Equations 32 (12) (2007) 1917–1939.
[50] R.M. Colombo, M. Herty, V. Sachers, On 2x2 conservation laws at a junction, SIAM J. Math. Anal. 40 (2) (2008) 605–622.
[51] L. Pan, Y. Zhu, Grey model prediction enhancement via Bernoulli equation with dynamic polynomial terms, Symmetry 17 (5) (2025) 713.
[52] R.M. Colombo, F. Marcellini, A mixed ODE–PDE model for vehicular traffic, Math. Methods Appl. Sci. 38 (7) (2015) 1292–1302.
[53] M.-C. Casabán, R. Company, V.N. Egorova, L. Jódar, A random free-boundary diffusive logistic differential model: Numerical analysis, computing and simulation, Math. Comput. Simulation (2024).
[54] B. de Jager, Symbolic computation in nonlinear control system modeling and analysis, in: Proceedings of the IEEE International Symposium on Computer Aided Control System Design, 1999, http://dx.doi.org/10.1109/CACSD.1999.808666.
[55] P. Jagers, The growth and stabilization of populations, Statist. Sci. 6 (3) (1991) 269–283, http://dx.doi.org/10.1214/ss/1177011694.
[56] M. Bronstein, Symbolic integration I: Transcendental functions, in: Algorithms and Computation in Mathematics, Vol. 1, Springer Berlin Heidelberg, 2005, http://dx.doi.org/10.1007/b138171.
[57] International Civil Aviation Organization, Aeronautical Information Regulation and Control (AIRAC), 2021, https://www2023.icao.int/airnavigation/information-management/Pages/AIRAC.aspx, (Accessed: February 9, 2026).
[58] D. Markovic, L. Borozan, On parameter estimation by nonlinear least squares in some special two-parameter exponential type models, Appl. Math. Inf. Sci. 9 (6) (2015) 2925.
[59] G. Zhang, D. Allaire, J. Cagan, Taking the guess work out of the initial guess: A solution interval method for least-squares parameter estimation in nonlinear models, J. Comput. Inf. Sci. Eng. 21 (2) (2021) 021011.
[60] T. Reitan, A. Petersen-Øverleir, Existence of the frequentistic estimate for power-law regression with a location parameter, with applications for making discharge rating curves, Stoch. Environ. Res. Risk Assess. 20 (2006) 445–453.
[61] H.P. Gavin, The Levenberg-Marquardt Algorithm for Nonlinear Least Squares Curve-Fitting Problems, Vol. 3, Department of Civil and Environmental Engineering Duke University, 2019, pp. 1–23.
[62] EUROCONTROL, Network manager ATFCM operations manual – edition MAINT-2 (valid from 18 june 2024), 2024, Retrieved from EUROCONTROL website.
[63] S. Węglarczyk, Kernel density estimation and its application, in: ITM Web of Conferences, Vol. 23, EDP Sciences, 2018, p. 00037.
[64] Y.-C. Chen, A tutorial on kernel density estimation and recent advances, Biostat. Epidemiol. 1 (1) (2017) 161–187.